3-21-2022

Nine Bright γ Doradus Variables Discovered with Ground-based Photometry

Gregory W. Henry
Tennessee State University

Francis C. Fekel
Tennessee State University

Michael H. Williamson
Tennessee State University

The Astronomical Journal, 163:180 (26pp), 2022 April https://doi.org/10.3847/1538-3881/ac540b

Nine Bright γ Doradus Variables Discovered with Ground-based Photometry

Gregory W. Henry, Francis C. Fekel[1], and Michael H. Williamson
Center of Excellence in Information Systems, Tennessee State University, 3500 John A. Merritt Boulevard, Box 9501, Nashville, TN 37209, USA;
gregory.w.henry@gmail.com, fekel@evans.tsuniv.edu, michael.h.williamson@gmail.com
Received 2021 October 1; revised 2022 January 28; accepted 2022 February 9; published 2022 March 21

Abstract

We have used precise photometric and high-dispersion spectroscopic observations to study nine candidate γ Doradus (γ Dor) stars, identified as optically variable comparison stars in our photometric studies of Sun-like stars. In this paper, we confirm these nine candidates as new γ Dor variables. All exhibit sinusoidal variability with amplitudes between 6 and 65 mmag in Johnson *B* and periods from 0.28 to 1.13 days. All lie in the same region of the H-R diagram as our previously confirmed γ Dor stars. Of the nine systems, one is a single-lined spectroscopic binary (SB1), two are double-lined spectroscopic binaries (SB2), and the remaining six are single stars. We present orbits for the three binary systems: HD 34415, HD 144839, and HD 182735. Their periods are 6400 days or 17.5 yr (adopted), 995 ± 7 days, and 1052.4 ± 0.2 days, respectively. We compare our photometric periods with those we derive for six of the nine stars observed with the Transiting Exoplanet Survey Satellite to strengthen the confirmation of these new γ Dor variables. Finally, because the distribution of γ Dor stars in the H-R diagram overlaps with the red edge of the δ Scuti (δ Sct) instability strip, we use our ground-based photometric results for the 73 γ Dor stars confirmed with our Automatic Photoelectric Telescopes over the past two decades to look at the incidence of hybrid δ Sct/γ Dor stars; these are highly valuable targets for asteroseismology.

Unified Astronomy Thesaurus concepts: Gamma Doradus variable stars (2101); Early-type stars (430); Fundamental parameters of stars (555); Stellar oscillations (1617); Radial velocity (1332); Spectroscopic binary stars (1557); Stellar photometry (1620); Period determination (1211)

Supporting material: machine-readable tables

1. Introduction

This is the 14th in our series of papers in which we examine the photometric and spectroscopic properties of candidate γ Dor variable stars. Our current total of 64 new, bright γ Dor field stars, along with original references to each discovery, are contained within the comprehensive catalog of Ibanoglu et al. (2018), who list 109 γ Dor stars confirmed as of 2017 January along with additional lists of 291 γ Dor candidates from the CoRoT mission (Baglin et al. 2006) and 523 candidates from Kepler (Borucki et al. 2010).

Kaye et al. (1999) gave an early definition of the γ Dor variables, based on a preliminary list of 13 confirmed members of the group, having spectral class from late A to early F, luminosity class V, IV–V, or IV, and exhibiting low-amplitude variability with one to five periods ranging from 0.4 to 3 days consistent with a driving mechanism of high-order, low-degree, nonradial gravity-mode pulsations. In their H-R diagram, these stars cluster in a small region on and somewhat above the main sequence that overlaps the cool edge of the δ Sct instability strip. A more recent list of 86 confirmed γ Dor stars by Henry et al. (2011) and the list of 109 stars in Ibanoglu et al. (2018) show that this early definition of the γ Dor variability class holds up quite well.

In this paper, we examine nine new γ Dor candidates that were discovered from their small-amplitude variability after they were selected for use as photometric comparison stars in our long-term program to measure brightness variability in Sun-like stars (e.g., Radick et al. 2018; Judge et al. 2020). Our Sun-like star program uses several of our 0.80 m two-channel Automatic Photoelectric Telescopes (APTs) at Fairborn Observatory, one of which (T8) is described in detail by Henry (1999). These telescopes deliver 0.0010–0.0015 mag precision for single observations and 0.0001–0.0002 mag for seasonal means. We found variability amplitudes in these nine new candidates ranging from 6 to 65 mmag.

We use our sample of γ Dor variables discovered or confirmed in our APT program in order to examine the incidence of hybrid δ Sct/γ Dor variability in the overlap region of the two instability strips and compare our ground-based incidence rate with the detection of hybrid pulsators discovered in recent space-based observations. As discussed in Pollard (2009), Grigahcene et al. (2010), Antoci et al. (2019), and Aerts (2021), the γ Dor, δ Sct, and especially the hybrid δ Sct/γ Dor pulsators offer tremendous potential for asteroseismology. The rich spectrum of pulsation frequencies identified in these stars acts as a probe of stellar structure and energy transport that enables a more detailed comparison with models of stellar structure.

2. The Sample

Table 1 lists the nine γ Dor candidates examined in this paper along with their basic properties. Once discovered to be variable in our Sun-like star program, these comparison stars were placed on the program of our T3 0.40 m APT for a year of higher-cadence observations. The nine stars have *V* magnitudes

[1] Visiting Astronomer, Kitt Peak National Observatory, National Optical Astronomy Observatory, operated by the Association of Universities for Research in Astronomy, Inc., under cooperative agreement with the National Science Foundation.

Table 1
Basic Properties of the γ Dor Stars

HD (1)	HIP (2)	Component (3)	V[a] (mag) (4)	$B-V$[a] (mag) (5)	π[b] (mas) (6)	Absolute Mag.[c] M_V (7)	Spectral Class (8)	Luminosity Class (9)	$v \sin i$ (km s^{-1}) (10)	Binary[d] (11)
6260	5024	⋯	8.22	0.34	8.4356 ± 0.0494	2.85	A9	dwarf	51	
19649	14696	⋯	7.64	0.39	8.9117 ± 0.0523	2.39	F2	subgiant	44	
28819	21246	⋯	7.78	0.33	9.5602 ± 0.0572	2.68	F0	dwarf	110	
34415	24693	A,B	8.38	0.37	8.2170 ± 0.0683					SB2
		A	8.47	0.30:		3.04	F0	dwarf:	41	
		B	11.17:	0.58:			G2:	dwarf	5:	
58431	36059	⋯	7.84	0.30	9.7168 ± 0.0581	2.78	F1	dwarf	34	
122928	68780	⋯	7.91	0.29	9.5110 ± 0.0653	2.80	F0	dwarf	69	
144839	78993	⋯	7.32	0.36	12.9166 ± 0.1426	2.88	F0	dwarf	100	SB1
182735	95271	A,B	7.39	0.36	12.0673 ± 0.1347					SB2
		A	7.52	0.33:		2.93	F1	dwarf	125	
		B	9.72:	0.62:			G2:	dwarf	3:	
210719	109614	⋯	7.14	0.35	12.6927 ± 0.0601	2.66	A9	dwarf	111	

Notes. A colon indicates greater uncertainty than usual.
[a] Single star values and combined values of binary components are from the Tycho-2 catalog converted to the Johnson system. For the individual binary components see the text.
[b] From the Gaia DR2 parallax catalog.
[c] Computed from the V magnitude in Col. 4 and the Gaia parallax in Col. 6.
[d] SB1 = single-lined binary, SB2 = double-lined binary.

within the range 7.14–8.47, have spectral classes from A9 to F2, and luminosity classes of dwarf or subgiant. We note that all nine stars appear in the revised Transiting Exoplanet Survey Satellite (TESS) Input Catalog (TIC; Stassun et al. 2019).

3. Spectroscopy

3.1. Observations

Between 2007 May and 2012 May we acquired high-dispersion spectrograms of our nine candidates listed in Table 1 at the Kitt Peak National Observatory (KPNO) with the coudé feed telescope and coudé spectrograph. The observations were obtained with three different CCD detectors. Initially, we used a Texas Instruments CCD to obtain spectrograms that were centered at 6430 Å, covered a wavelength range of 84 Å, and had a two-pixel resolution of 0.21 Å. For our 2008 September observing run, the TI CCD was unavailable, so we used a Tektronics CCD identified as T1KA. The spectrum was centered at 6400 Å, the wavelength coverage increased to 172 Å, but the resolution decreased to 0.35 Å. Beginning in 2010 September, after the TI CCD was retired, we acquired our spectrograms with a CCD made by Semiconductor Technology Associates and given the designation STA2. With that CCD the spectra were again centered at 6430 Å, and the wavelength range was increased to 336 Å. The spectrograph slit was set so that the STA2 spectra had the same resolution as those acquired with the TI CCD. However, the resolution of the STA2 spectra was degraded at both ends. The typical signal-to-noise ratio of our KPNO spectra is about 125.

We obtained additional spectrograms from 2011 July through 2021 September with the TSU 2 m Automatic Spectroscopic Telescope (AST) and fiber-fed echelle spectrograph, located at Fairborn Observatory in southeastern Arizona (Eaton & Williamson 2007). Initially, the detector was a 2048 × 4096 SITe ST-002A CCD with 15 μm pixels. The resulting echelle spectrograms have 21 orders that span the wavelength range 4920–7100 Å and have an average resolution of 0.17 Å. The typical signal-to-noise ratio is ∼50 at 6000 Å. Eaton & Williamson (2007) have described the general reduction of the raw spectra and their wavelength calibration. In the late summer of 2011, we replaced the SITe CCD and its dewar with a new dewar and a Fairchild 486 CCD having a 4096 × 4096 array of 15 μm pixels. The new spectrograms have 48 orders ranging from 3800 to 8260 Å. For all stars except HD 182735, we used a 200 μm fiber, which gave a resolution of 0.24 Å. For HD 182735, we used a 365 μm fiber, which resulted in a resolution of 0.4 Å. Fekel et al. (2013) provide additional information about the new setup.

3.2. Analyses

3.2.1. Basic Properties

Our KPNO and Fairborn spectrograms were used to derive the basic properties of our program stars listed in Table 1. The properties of the single stars were determined in a relatively straightforward manner (Henry et al. 2001). The spectral class of each star given in column 8 was estimated from its individual red-wavelength KPNO spectrograms by comparing them with the spectrograms of several slowly rotating late A and early F stars from the list of Abt & Morrell (1995). The luminosity classes in column 9 were determined from the Tycho-2 magnitudes (Hog et al. 2000) converted to Johnson B and V and the Gaia DR2 parallaxes (Gaia Collaboration et al. 2018) in comparison with Yonsei–Yale evolutionary models (Demarque et al. 2004). Because the luminosity classes were not estimated from the spectra, we have not identified them in column 9 by Roman numerals but rather by the words "dwarf" or "subgiant."

The stars HD 34415 (Figure 1) and HD 182735 (Figure 2) are double-lined binaries, so determining individual magnitudes and colors of the components in Table 1 is more involved. For those binaries we estimated a V magnitude difference via the spectrum addition method described in Fekel et al. (2003). That procedure results in a continuum luminosity

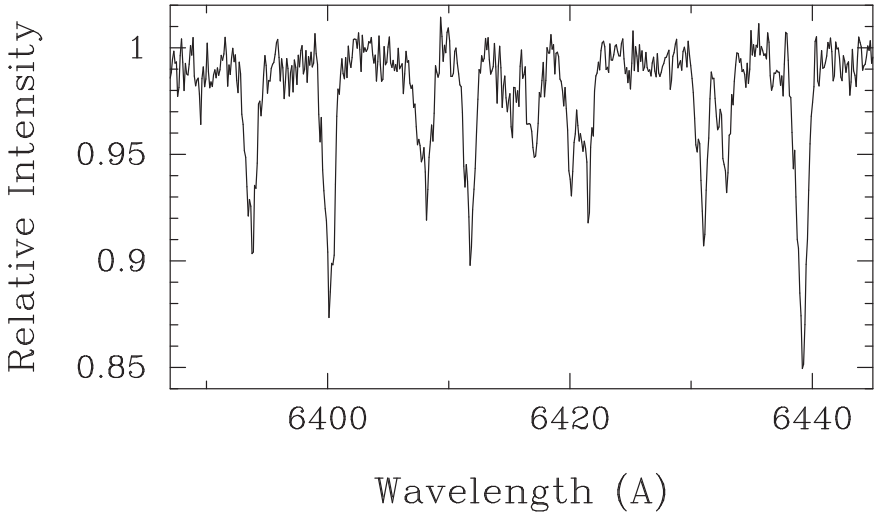

Figure 1. Spectrum of HD 34415 in the 6430 Å region, which shows the composite profiles of the lines. Component A has the stronger broad lines. The sharp and much weaker lines of component B sit near the center of the broader features.

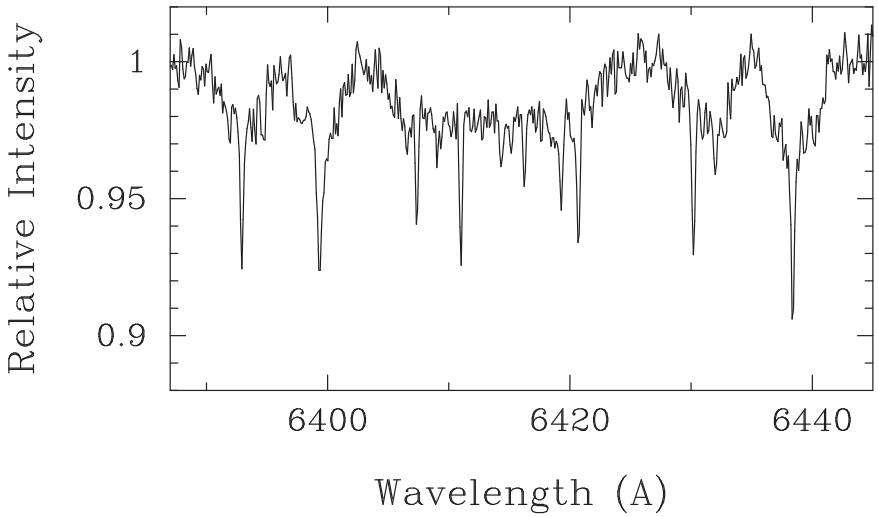

Figure 2. Spectrum of HD 182735 in the 6430 Å region, which shows the composite profiles of the lines. Component A is the broad-lined star. Component B is the narrow-lined star that is positioned near the center of the broad-lined component.

ratio, which is converted into a minimum magnitude difference when the secondary has a later spectral type than the primary. For a large spectral type difference, such as the components of HD 34415 and HD 182735, the continuum luminosity ratio must be adjusted for the difference in spectral types before estimating a magnitude difference.

We determined the average $v \sin i$ values for each star, given in Table 1, column 10, from the rotational broadening fits described below. Because the stars are pulsating, the line profiles have intrinsic variability in their shape to a greater or lesser extent. The estimated uncertainty we assigned, which increases as the projected rotational velocity becomes larger, is greater than the formal uncertainty. For a $v \sin i$ of 100, our estimated uncertainty is 4 km s^{-1}; for rotational velocities near 50 km s^{-1}, it is 2 km s^{-1}; and for values below about 30 km s^{-1}, it is 1 km s^{-1}. For the composite spectrum binaries, the narrow-lined components are affected by the line-profile variations of the broad-lined components, and so the uncertainties of the rotational velocities are greater than the 1 km s^{-1} estimate noted above. A colon next to the value in column 10 indicates the larger uncertainty.

Fekel et al. (2003) furnish the details of the reduction and analysis of our KPNO spectra and provide information about the uncertainties of the various measurements. Briefly, we determined radial velocities from those spectra by cross-correlation, measuring the regions around five lines for the more slowly rotating stars but, because of the extensive line blending, just one or two line regions for the most rapidly rotating stars. The radial velocities adopted for the standard stars used in the correlations are from Scarfe et al. (1990).

Fekel et al. (2009) give a general description of the Fairborn AST spectrum analysis. In summary, we measured radial velocities of 168 mostly neutral Fe lines from a solar-type star list that covered the 4920–7120 Å region. Because of the extensive line broadening of most stars, we used a rotational broadening function (Fekel & Griffin 2011; Lacy & Fekel 2011) to fit the lines. To place the velocities on the velocity system of Scarfe et al. (1990), we added 0.3 km s^{-1} to the average velocity of each AST observation acquired before 2011 September with the old CCD. Velocities obtained with the new CCD have a slightly different zero-point, and so, to

maintain the Scarfe zero-point, we add 0.6 km s^{-1} to the new CCD velocities.

For the γ Dor pulsators, the uncertainties of our radial velocity measurements vary because they depend on the amount of line broadening and, to a lesser extent, the line asymmetries resulting from pulsation. Stars with $v \sin i$ of 100 km s^{-1} or more have velocity uncertainties of about 1.5 km s^{-1}, while those with $v \sin i$ values of about 50 km s^{-1} or less have uncertainties of about 0.4 km s^{-1}. Although the lines for the G-star secondaries of the two double-lined binaries have little rotational broadening, the lines are quite weak, typically being only 2%–4% deep and are always blended with the broad-lined γ Dor pulsators, so we estimate velocity uncertainties of 0.7 km s^{-1} from their orbital fits.

The individual radial velocities for the stars that do not show orbital motion are listed in Table 2. If the spectral features are significantly asymmetric, that fact is mentioned in column 5.

3.3. Spectroscopic Orbits

Three of our stars, HD 34415, HD 144839, and HD 182735, are spectroscopic binaries, and we obtain orbits for all three systems. HD 34415 is a double-lined binary that shows significant long-term orbital motion, for which we have obtained a preliminary orbit. Of the other two systems, HD 144839 is single-lined while HD 182735 is double-lined; both are found to have periods near 1000 days.

For each binary, we first identified an approximate orbital period with the computer program PDFND, which uses the least-string method as implemented by T. J. Deeming (Bopp et al. 1970). Initial orbits for individual components were then determined with BISP (Wolfe et al. 1967), which solves for the orbital elements with the Wilsing–Russell Fourier analysis method. We next refined those elements with SB1, a program that utilizes differential corrections (Barker et al. 1967). For the double-lined binaries, we obtained a solution with SB2, a slightly modified version of SB1.

3.3.1. HD 34415

As noted earlier, the spectrum of HD 34415 (Figure 1) is composite, consisting of very weak, narrow lines of the secondary sitting completely inside the broader and significantly stronger lines of the primary. Our velocities of both components show definite orbital motion during the 12.5 yr of observation but certainly do not cover a full orbital cycle. Nevertheless, we attempted to obtain preliminary orbital elements. We initially examined the velocities of the secondary, which have the narrower lines and larger velocity amplitude, and computed elements for periods ranging from 6000 to 12,000 days in steps of 1000 days. Those seven solutions provide reasonable fits to the velocities but significantly different orbits. We next obtained orbital solutions of the primary, adopting values of the period, time of periastron passage, the argument of periastron plus 180°, and eccentricity derived from each corresponding solution of the secondary. Searching the literature, we found three additional radial velocities of the primary that had been obtained by Nordström et al. (1997) at the observatories of the Center for Astrophysics (CfA) about 20 yr earlier than the start of our observations. Although the velocities of the primary are affected by the pulsational changes of the line shape, and the zero-point of the Nordström et al. (1997) velocity system may be somewhat

Table 2
Individual Radial Velocities of Single Stars

HD	Helio. Julian Date HJD–2,400,000	Radial Velocity (km s^{-1})	Source[a]	Comments
(1)	(2)	(3)	(4)	(5)
6260	54729.837	5.2	KPNO	
	54730.845	4.4	KPNO	Asymmetric lines
	55094.911	7.0	KPNO	
	56673.629	4.7	FO	Asymmetric lines
	56674.655	0.9	FO	Asymmetric lines
	56675.686	1.6	FO	Asymmetric lines
	56676.685	2.3	FO	
	56677.641	4.5	FO	Asymmetric lines
	56678.696	6.1	FO	Asymmetric lines
	56706.685	3.8	FO	Asymmetric lines
	56782.974	1.4	FO	
	56810.923	2.7	FO	Asymmetric lines
	56832.843	3.0	FO	Asymmetric lines
	56834.838	1.6	FO	
	56836.883	3.0	FO	Asymmetric lines
	56839.842	4.1	FO	
	56900.673	3.7	FO	Asymmetric lines
	56926.603	4.0	FO	
	56933.733	2.9	FO	Asymmetric lines
	56935.642	2.3	FO	Asymmetric lines
	56942.758	4.7	FO	Asymmetric lines
	56944.669	4.1	FO	
	59391.786	2.7	FO	
	59392.823	3.6	FO	
	59447.779	3.2	FO	Asymmetric lines
	59448.704	2.3	FO	
	59449.669	5.5	FO	
	59466.705	4.9	FO	Asymmetric lines
	59467.658	4.6	FO	
	59469.753	2.4	FO	
	59470.624	4.6	FO	Asymmetric lines
	59471.628	1.8	FO	Asymmetric lines
	59472.610	2.1	FO	
	59473.609	2.8	FO	Asymmetric lines
	59478.664	1.7	FO	Asymmetric lines
	59479.606	4.6	FO	Asymmetric lines
19649	54368.954	12.6	KPNO	
	54731.931	12.4	KPNO	
	54733.921	14.3	KPNO	
	56674.632	12.2	FO	Asymmetric lines
	56675.619	12.0	FO	Asymmetric lines
	56676.619	11.8	FO	Asymmetric lines
	56677.603	11.1	FO	Asymmetric lines
	56678.630	12.8	FO	Asymmetric lines
	56702.684	13.6	FO	
	56941.894	14.9	FO	
	56989.746	15.1	FO	Asymmetric lines
28819	54368.973	26.8	KPNO	
	54734.982	27.2	KPNO	
	56674.611	24.9	FO	Asymmetric lines
	56675.647	24.2	FO	
	56676.647	24.9	FO	
	56677.658	26.1	FO	Asymmetric lines
	56678.658	25.6	FO	
	56698.744	26.4	FO	
	56707.766	23.7	FO	Asymmetric lines
	56900.901	22.4	FO	
	56933.756	19.0	FO	
	56944.727	24.5	FO	
	56990.756	23.9	FO	
58431	54583.655	10.1	KPNO	

Table 2
(Continued)

HD	Helio. Julian Date HJD–2,400,000	Radial Velocity (km s^{-1})	Source[a]	Comments
(1)	(2)	(3)	(4)	(5)
	54586.622	10.2	KPNO	
	54950.656	10.2	KPNO	
	56674.624	9.5	FO	
	56675.660	9.4	FO	
	56676.659	10.3	FO	
	56677.691	9.5	FO	
	56678.671	10.0	FO	
	56700.857	9.2	FO	
	56740.770	10.4	FO	
	56772.709	9.0	FO	
	56932.015	10.6	FO	
	56971.824	10.9	FO	
122928	54222.832	−23.0	KPNO	
	54223.834	−21.5	KPNO	
	54263.721	−24.8	KPNO	
	54267.736	−23.3	KPNO	
	54585.884	−20.8	KPNO	
	55314.798	−22.6	KPNO	
	56680.904	−22.6	FO	Asymmetric lines
	56699.883	−23.0	FO	
	56707.980	−24.2	FO	Asymmetric lines
	56724.945	−24.0	FO	Asymmetric lines
	56742.943	−24.7	FO	
	56751.914	−24.5	FO	
	56756.931	−24.9	FO	Asymmetric lines
	56771.894	−21.8	FO	
	56785.891	−22.8	FO	
	56808.763	−23.5	FO	
	57046.010	−22.4	FO	
	57065.031	−22.3	FO	
	57098.926	−23.9	FO	
	57355.035	−23.0	FO	
	57414.869	−22.6	FO	
	57436.890	−24.6	FO	
	57463.814	−22.8	FO	
	57482.870	−24.5	FO	
	57496.982	−23.4	FO	
	57508.963	−21.8	FO	
	57524.919	−21.3	FO	
	57535.724	−23.9	FO	Asymmetric lines
210719	54367.724	22.5	KPNO	Asymmetric lines
	54731.756	23.6	KPNO	Asymmetric lines
	55096.759	27.4	KPNO	Asymmetric lines
	56762.995	15.6	FO	Asymmetric lines
	56764.995	19.2	FO	
	56768.969	13.7	FO	
	56769.990	15.8	FO	Asymmetric lines
	56770.971	21.3	FO	
	56771.972	16.9	FO	
	56772.962	21.0	FO	
	56773.956	21.1	FO	
	56775.959	18.7	FO	Asymmetric lines
	56776.986	19.7	FO	
	56777.948	12.1	FO	Asymmetric lines
	56778.967	16.3	FO	
	56779.960	17.2	FO	
	56780.941	17.2	FO	
	56781.953	16.2	FO	Asymmetric lines
	56782.934	18.1	FO	
	56783.947	16.5	FO	Asymmetric lines
	56785.943	18.7	FO	

Table 2
(Continued)

HD	Helio. Julian Date HJD–2,400,000	Radial Velocity (km s^{-1})	Source[a]	Comments
(1)	(2)	(3)	(4)	(5)
	56786.930	21.5	FO	Asymmetric lines
	56787.922	18.7	FO	
	56789.917	16.2	FO	Asymmetric lines
	56790.914	19.3	FO	
	56822.836	19.9	FO	
	56900.807	22.2	FO	
	56940.688	21.0	FO	
	57130.981	18.8	FO	
	57184.911	20.1	FO	
	57493.984	19.5	FO	
	57521.956	15.4	FO	
	57553.857	15.5	FO	
	57616.793	21.7	FO	
	57663.657	24.1	FO	Asymmetric lines
	57706.640	16.8	FO	Asymmetric lines
	57855.996	19.2	FO	
	57906.971	17.2	FO	
	57972.906	19.8	FO	Asymmetric lines
	58018.667	16.4	FO	Asymmetric lines
	58059.780	15.7	FO	
	58110.633	22.7	FO	
	58229.989	16.2	FO	
	58275.888	20.4	FO	
	58388.637	16.9	FO	Asymmetric lines
	58439.635	19.4	FO	
	58766.677	18.5	FO	
	59021.971	21.9	FO	
	59134.841	17.1	FO	
	59181.628	17.3	FO	
	59321.986	13.2	FO	

Note.
[a] KPNO = Kitt Peak National Observatory, FO = Fairborn Observatory.

different than ours, we included those velocities in the primary solution but with zero weight to see where they fit best in phase. Their addition resulted in a best period of 6400 days. Thus, with the period fixed at 6400 days, we obtained a solution of our secondary velocities. Then, as we did previously, we acquired a solution of the primary solving only for its semiamplitude and center-of-mass velocity. From the inverse ratio of the variances of the solutions of the primary and secondary, we assigned a weight of 0.4 to each KPNO and Fairborn velocity of the primary but continued to give the Nordström et al. (1997) velocities zero weight. We adopted a weight of 1.0 for each secondary velocity. As our final solution, we obtained a simultaneous solution of the two components with the period fixed at 6400 days and all the other elements allowed to vary. Table 3 lists the observations and velocities used in this final solution. The resulting orbital elements are given in Table 4, and the phased velocities are compared with the computed velocity curves in Figure 3.

3.3.2. HD 144839

The spectrum of HD 144839 shows only a single set of broad lines. A period search of all our velocities resulted in an orbital period of 983 days. We then obtained orbital elements of the

Table 3
Radial Velocity Observations of HD 34415

Hel. Julian Date HJD−2,400,000	Phase	RV_A (km s^{-1})	$(O-C)_A$ (km s^{-1})	Wt_A	RV_B (km s^{-1})	$(O-C)_B$ (km s^{-1})	Wt_B	Source[a]
46820.669	0.466	36.1	0.3	0.0	...	...	...	CfA
47218.622	0.528	35.1	0.0	0.0	...	...	...	CfA
47849.788	0.627	34.0	0.2	0.0	...	...	...	CfA
54730.999	0.702	32.2	−0.4	0.4	35.3	−0.5	1.0	KPNO
54732.947	0.702	31.2	−1.4	0.4	35.4	−0.4	1.0	KPNO
55098.941	0.760	30.9	−0.6	0.4	36.6	−1.1	1.0	KPNO
56674.599	0.006	30.6	0.4	0.4	38.8	−1.1	1.0	FO
56675.635	0.006	30.8	0.6	0.4	40.8	1.0	1.0	FO
56676.634	0.006	30.8	0.5	0.4	39.9	0.1	1.0	FO
56677.677	0.006	30.3	0.0	0.4	40.2	0.4	1.0	FO
56678.646	0.006	30.4	0.1	0.4	39.5	−0.3	1.0	FO
56700.690	0.010	32.7	2.2	0.4	39.4	0.0	1.0	FO
56754.678	0.018	31.9	0.8	0.4	37.7	−0.7	1.0	FO
56897.950	0.041	31.8	−0.9	0.4	36.6	1.0	1.0	FO
56934.843	0.046	33.9	0.8	0.4	35.1	0.2	1.0	FO
56966.777	0.051	33.0	−0.4	0.4	34.6	0.2	1.0	FO
57283.860	0.101	37.8	1.9	0.4	29.7	−0.5	1.0	FO
57333.949	0.109	35.7	−0.4	0.4	30.1	0.3	1.0	FO
57384.664	0.117	35.7	−0.7	0.4	29.7	0.3	1.0	FO
57422.806	0.123	36.9	0.4	0.4	28.8	−0.4	1.0	FO
57446.739	0.126	37.4	0.8	0.4	27.6	−1.4	1.0	FO
57473.702	0.131	35.1	−1.6	0.4	28.3	−0.6	1.0	FO
57648.884	0.158	37.6	0.5	0.4	27.3	−0.9	1.0	FO
57676.788	0.162	37.1	0.0	0.4	28.2	0.1	1.0	FO
57702.979	0.167	38.6	1.4	0.4	27.6	−0.4	1.0	FO
57732.920	0.171	35.8	−1.4	0.4	29.3	1.4	1.0	FO
57766.790	0.176	36.1	−1.2	0.4	28.4	0.5	1.0	FO
57787.776	0.180	39.1	1.8	0.4	27.4	−0.4	1.0	FO
57827.710	0.186	39.3	2.0	0.4	26.9	−0.9	1.0	FO
57864.634	0.192	36.2	−1.2	0.4	27.6	−0.1	1.0	FO
57972.972	0.209	37.2	−0.2	0.4	28.3	0.7	1.0	FO
58014.844	0.215	36.8	−0.6	0.4	27.8	0.2	1.0	FO
58040.783	0.219	39.0	1.6	0.4	26.6	−1.0	1.0	FO
58073.837	0.224	36.4	−1.0	0.4	28.6	1.0	1.0	FO
58145.596	0.236	38.5	1.1	0.4	28.4	0.8	1.0	FO
58206.654	0.245	37.6	0.2	0.4	26.6	−1.0	1.0	FO
58369.913	0.271	37.8	0.5	0.4	27.3	−0.5	1.0	FO
58417.843	0.278	37.4	0.1	0.4	28.1	0.3	1.0	FO
58465.685	0.286	37.0	−0.3	0.4	28.6	0.7	1.0	FO
58527.786	0.295	37.7	0.5	0.4	28.2	0.2	1.0	FO
58575.670	0.303	35.0	−2.2	0.4	28.5	0.5	1.0	FO
58722.942	0.326	37.6	0.6	0.4	28.3	0.0	1.0	FO
58785.923	0.336	37.1	0.1	0.4	29.1	0.7	1.0	FO
58836.606	0.344	35.7	−1.2	0.4	29.6	1.1	1.0	FO
58897.802	0.353	37.1	0.3	0.4	29.1	0.5	1.0	FO
59098.923	0.385	36.7	0.1	0.4	29.5	0.5	1.0	FO
59152.042	0.393	36.7	0.2	0.4	27.5	−1.7	1.0	FO
59202.608	0.401	38.0	1.6	0.4	29.8	0.5	1.0	FO
59251.742	0.409	36.5	0.1	0.4	28.6	−0.8	1.0	FO
59306.685	0.417	35.9	−0.4	0.4	28.7	−0.8	1.0	FO

Note.
[a] CfA = Center for Astrophysics, KPNO = Kitt Peak National Observatory, FO = Fairborn Observatory.
(This table is available in its entirety in machine-readable form.)

Fairborn Observatory velocities alone and refined that result. The KPNO velocities are more limited in number and have poor phase coverage, so we obtained an orbital solution of those velocities by adopting the Fairborn elements but allowed the center-of-mass velocity to vary. The center-of-mass velocities of the two solutions agreed to within their uncertainties. From the inverse ratio of the variances of the two solutions, we assigned weights of 1.0 to the Fairborn velocities and 0.3 to those from KPNO. Using the velocities from both observatories, we then obtained a final orbital solution. The observing times and velocities are listed in Table 5, while our final orbital elements are given in Table 6. A phase plot of velocities compared to the predicted orbit is shown in Figure 4.

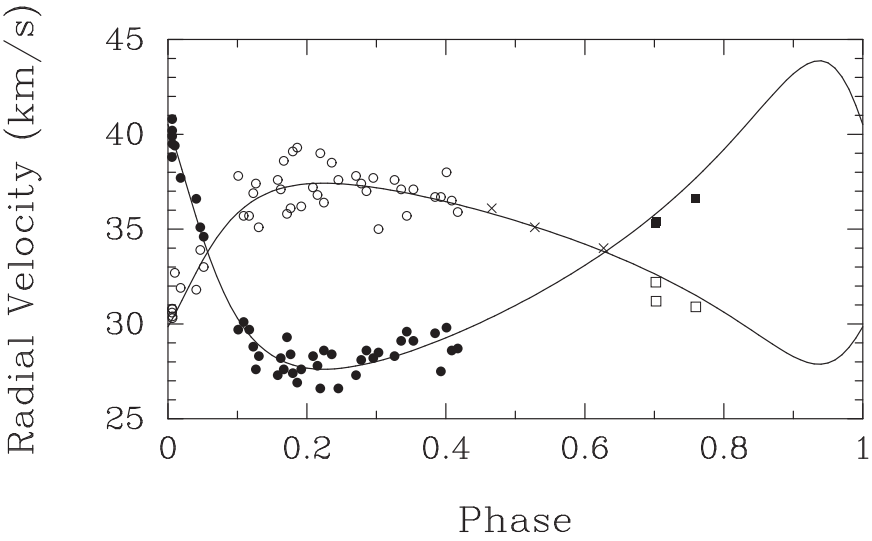

Figure 3. A plot of the HD 34415 radial velocities compared with the computed velocity curves (solid lines). Each CfA velocity is represented by a cross. The squares correspond to KPNO velocities and the circles to those of Fairborn Observatory, with open symbols representing the primary and solid symbols the secondary. Phase zero is a time of periastron passage. This preliminary orbit for HD 34415 has an orbital period of 6400 days and a moderate eccentricity of 0.43.

Table 4
HD 34415 Spectroscopic Orbital Elements and Related Parameters

Parameter	Value
P (days)	6400 (adopted)
T (HJD)	2,456,637.2 ± 66.3
e	0.409 ± 0.021
ω (deg)	234.1 ± 5.4
K_A (km s^{-1})	4.77 ± 0.33
K_B (km s^{-1})	8.14 ± 0.42
γ (km s^{-1})	33.79 ± 0.23
$a_A \sin i$ (10^6 km)	383.3 ± 26.4
$a_B \sin i$ (10^6 km)	653.3 ± 34.3
$m_A \sin^3 i$ ($M_\odot$)	0.683 ± 0.081
$m_B \sin^3 i$ ($M_\odot$)	0.401 ± 0.051
Standard error of an observation of unit weight (km s^{-1})	0.7

3.3.3. HD 182735

As seen in Figure 2, the spectrum of HD 182735 is double lined, consisting of a very broad primary component and a very narrow secondary. We first made a period search of the secondary velocities and determined a period of 1051 days. A single-lined binary solution resulted in an orbital period of 1052.4 days and a high eccentricity of 0.728. The lines of the primary are very broad, having a $v \sin i$ of 125 km s^{-1}, and change shape because of γ Dor pulsation, so to obtain an orbital solution of the primary, we adopted the values of the period, time of periastron passage, the argument of periastron plus 180°, and eccentricity from our solution of the secondary. Thus, for our solution of the primary velocities, only the semiamplitude and center-of-mass velocity were allowed to vary. Because of the very significant difficulties in obtaining accurate measurements of the primary velocities, it is not particularly surprising that the center-of-mass velocity found for the primary is somewhat different, 1.8 km s^{-1} more negative, than that for the secondary orbit. To obtain a simultaneous solution of the two components, from the inverse ratio of the variances of the two single star solutions, we assigned weights of 1.0 to the secondary velocities and 0.06 to all primary velocities and also added 1.8 km s^{-1} to all the primary velocities. Table 7 lists our radial velocities. The final orbital elements are given in Table 8, and a phase plot of the velocities compared with the computed velocity curves is shown in Figure 5.

3.4. Other Velocity Variability

3.4.1. Pulsation Period Search

The radial velocity cadence for our nine γ Dor candidates ranges from one observation per day for a few days down to one observation every few months, so the radial velocities are not well suited for the detection of short-period pulsations. Nevertheless, we examined our radial velocities of all nine stars to determine whether the pulsation periods found in the photometric data (discussed below) could be detected in the radial velocities. First, we phased the velocities for the six single stars to each of the photometric periods found in each star; we found no evidence for radial velocity variability at any of the photometric periods. Next, for the three binary stars, we phased the residuals of the Fairborn velocities from the orbital fit of each primary component to the photometric periods identified in each of those stars. Again, we found no evidence for radial velocity variability at any of the photometric periods. These negative results are not particularly surprising, because Mathias et al. (2004) have pointed out that the dominant frequency identified in the photometry will not necessarily be the same one detected in the spectroscopy because the two techniques are most sensitive to different modes of pulsation.

Finally, we executed a period search of the velocity data for HD 6260, HD 122928, and HD 210719, the three single stars for which we have at least 15 observations, and also searched the residual velocities of the orbital fits for the primaries of the binaries HD 34415, HD 144839, and HD 182735. We fit sine curves to the data, phasing the velocities with trial periods from 0.19 to 5.0 days, a range that covers the periods found photometrically in γ Dor stars. The trial period step size was 0.00001 day up to 3.0 days and 0.001 day for periods greater than 3.0 days. The trial period with the smallest squared sum of the residuals was identified as the most likely period. A phase

Table 5
Radial Velocity Observations of HD 144839

Hel. Julian Date HJD−2,400,000	Phase	RV (km s^{-1})	$(O-C)$ (km s^{-1})	Wt	Source[a]
54585.948	0.841	−33.1	0.1	0.3	KPNO
54586.824	0.842	−35.0	−1.8	0.3	KPNO
54730.608	0.987	−24.4	2.2	0.3	KPNO
54731.594	0.988	−24.2	2.3	0.3	KPNO
54732.608	0.989	−26.1	0.4	0.3	KPNO
54734.614	0.991	−27.7	−1.3	0.3	KPNO
54949.945	0.207	−23.6	1.9	0.3	KPNO
55004.846	0.262	−28.7	−1.6	0.3	KPNO
55313.928	0.573	−37.7	−2.6	0.3	KPNO
55314.847	0.574	−33.7	1.4	0.3	KPNO
55366.793	0.626	−30.8	4.8	0.3	KPNO
55370.803	0.630	−34.8	0.9	0.3	KPNO
55680.887	0.941	−27.8	0.9	0.3	KPNO
55731.797	0.993	−26.5	−0.2	0.3	KPNO
55732.829	0.994	−26.7	−0.4	0.3	KPNO
55733.878	0.995	−28.4	−2.2	0.3	KPNO
55734.852	0.996	−23.0	3.2	0.3	KPNO
55735.879	0.997	−22.9	3.2	0.3	KPNO
56674.998	0.940	−28.7	0.1	1.0	FO
56675.960	0.941	−28.6	0.1	1.0	FO
56676.983	0.942	−29.7	−1.0	1.0	FO
56677.976	0.943	−30.5	−1.9	1.0	FO
56704.034	0.969	−27.8	−0.5	1.0	FO
56729.001	0.995	−24.0	2.2	1.0	FO
56751.866	0.018	−23.2	2.2	1.0	FO
56775.954	0.042	−23.7	0.9	1.0	FO
56804.856	0.071	−25.3	−1.2	1.0	FO
56827.915	0.094	−25.0	−1.1	1.0	FO
56902.707	0.169	−25.2	−0.5	1.0	FO
57015.044	0.282	−27.6	0.2	1.0	FO
57060.004	0.327	−26.5	2.7	1.0	FO
57106.896	0.374	−27.9	2.7	1.0	FO
57177.977	0.446	−31.0	1.5	1.0	FO
57413.046	0.682	−34.6	1.3	1.0	FO
57447.866	0.717	−35.9	−0.2	1.0	FO
57475.001	0.744	−34.7	0.8	1.0	FO
57493.820	0.763	−33.1	2.1	1.0	FO
57505.958	0.775	−32.5	2.5	1.0	FO
57520.782	0.790	−36.5	−1.8	1.0	FO
57535.807	0.805	−34.9	−0.6	1.0	FO
57544.883	0.814	−34.0	0.1	1.0	FO
57577.818	0.847	−32.2	0.8	1.0	FO
57628.660	0.899	−30.7	0.1	1.0	FO
57747.021	0.017	−25.6	−0.2	1.0	FO
57780.959	0.052	−25.6	−1.2	1.0	FO
57788.017	0.059	−24.8	−0.5	1.0	FO
57817.927	0.089	−24.3	−0.4	1.0	FO
57848.793	0.120	−22.1	1.9	1.0	FO
57864.731	0.136	−24.4	−0.3	1.0	FO
57885.971	0.157	−24.8	−0.4	1.0	FO
57901.870	0.173	−24.0	0.7	1.0	FO
57917.900	0.189	−26.2	−1.1	1.0	FO
57981.761	0.253	−26.9	0.0	1.0	FO
57982.740	0.254	−28.4	−1.5	1.0	FO
58027.633	0.299	−29.1	−0.8	1.0	FO
58142.962	0.415	−31.9	−0.2	1.0	FO
58153.921	0.426	−30.1	1.9	1.0	FO
58159.934	0.432	−31.9	0.3	1.0	FO
58179.922	0.452	−32.4	0.3	1.0	FO
58210.798	0.483	−33.2	0.2	1.0	FO
58223.964	0.497	−34.3	−0.6	1.0	FO
58248.757	0.522	−35.1	−0.9	1.0	FO
58255.935	0.529	−35.6	−1.3	1.0	FO
58267.946	0.541	−34.3	0.2	1.0	FO
58287.898	0.561	−37.1	−2.2	1.0	FO
58510.962	0.785	−35.1	−0.3	1.0	FO
58595.000	0.869	−32.7	−0.6	1.0	FO
58624.924	0.900	−30.0	0.8	1.0	FO
58660.859	0.936	−31.8	−2.8	1.0	FO
58881.951	0.158	−23.3	1.1	1.0	FO
58968.977	0.245	−28.5	−1.9	1.0	FO
58981.871	0.258	−27.3	−0.3	1.0	FO
59205.039	0.482	−34.9	−1.5	1.0	FO
59219.008	0.496	−34.2	−0.5	1.0	FO
59257.911	0.536	−34.0	0.5	1.0	FO
59302.779	0.581	−34.9	0.3	1.0	FO
59315.003	0.593	−37.1	−1.8	1.0	FO
59324.946	0.603	−36.3	−0.9	1.0	FO
59333.900	0.612	−36.3	−0.8	1.0	FO
59340.778	0.619	−34.4	1.2	1.0	FO
59348.658	0.627	−36.7	−1.1	1.0	FO

Note.
[a] KPNO = Kitt Peak National Observatory, FO = Fairborn Observatory.

(This table is available in its entirety in machine-readable form.)

Table 6
HD 144839 Spectroscopic Orbital Elements and Related Parameters

Parameter	Value
P (days)	995.3 ± 6.7
T (HJD)	2,456,734.4 ± 43.4
e	0.160 ± 0.045
ω (deg)	310.5 ± 17.2
K (km s^{-1})	5.97 ± 0.27
γ (km s^{-1})	−30.51 ± 0.20
$a \sin i$ (10^6 km)	80.7 ± 3.7
f(m) ($M_\odot$)	0.0211 ± 0.0029
Standard error of an observation of unit weight (km s^{-1})	1.3

diagram of this best period was created, and the plot was visually examined to determine the likely reality of the period. Only in the case of HD 6260 is there a possible periodicity in the γ Dor range (see Section 5.1 below).

4. Photometry

4.1. APT Observations

The follow-up photometric observations of the nine γ Dor candidates reported in this paper were acquired between 2006 December 1 and 2008 June 30 with the T3 0.40 m APT located at Fairborn Observatory. This APT has a single-channel photometer equipped with a temperature-stabilized EMI 9924B photomultiplier tube that measures count rates successively through Johnson B and V filters. Each candidate is measured in the following sequence, termed a group observation: *K, S, C, V, C, V, C, V, C, S, K*, in which K is a check star, C is a comparison star, V is the program (candidate γ Dor) star, and S is a sky reading. Table 9 lists the comparison and check stars used for each program star as well as the APT (T8, T10,

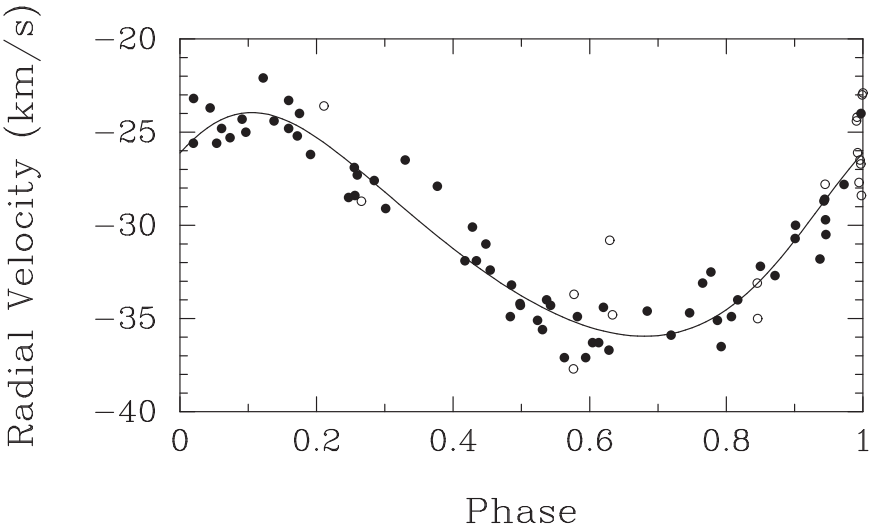

Figure 4. A plot of the HD 144839 radial velocities (Solid circles = Fairborn Observatory and open circles = KPNO) compared with the computed velocity curve (solid line). Phase zero is a time of periastron passage. The binary has an orbital period of 995 days and a modest eccentricity of 0.16.

Table 7
Radial Velocity Observations of HD 182735

Hel. Julian Date HJD−2,400,000	Phase	RV_A (km s^{-1})	$(O-C)_A$ (km s^{-1})	Wt_A	RV_B (km s^{-1})	$(O-C)_B$ (km s^{-1})	Wt_B	Source[a]
54367.647	0.376	−17.7	0.0	0.06	−24.1	−0.2	1.00	KPNO
54586.000	0.583	−16.8	4.3	0.06	−18.6	0.4	1.00	KPNO
54731.701	0.722	−20.2	3.5	0.06	−15.9	−0.6	1.00	KPNO
54732.699	0.722	−19.8	4.0	0.06	−16.0	−0.7	1.00	KPNO
55003.863	0.980	−32.2	−0.1	0.06	−4.4	−1.0	1.00	KPNO
55314.997	0.276	−12.7	3.2	0.06	−26.7	−0.3	1.00	KPNO
55365.895	0.324	−19.8	−3.0	0.06	−25.5	−0.4	1.00	KPNO
55369.896	0.328	−16.6	0.3	0.06	−25.9	−0.9	1.00	KPNO
55681.972	0.625	−22.4	−0.6	0.06	−19.1	−1.1	1.00	KPNO
55731.912	0.672	−20.9	1.8	0.06	−17.5	−0.8	1.00	KPNO
55734.906	0.675	−20.7	2.1	0.06	−17.5	−0.8	1.00	KPNO
55743.665	0.683	−19.3	3.6	0.06	−17.1	−0.7	1.00	FO
55756.666	0.695	−23.6	−0.4	0.06	−16.7	−0.6	1.00	FO
55846.789	0.781	−25.2	0.0	0.06	−14.0	−0.7	1.00	FO
55847.745	0.782	−27.0	−1.8	0.06	−12.7	0.5	1.00	FO
55848.673	0.783	−27.3	−2.1	0.06	−12.8	0.4	1.00	FO
55853.659	0.788	−27.0	−1.7	0.06	−12.9	0.1	1.00	FO
55855.656	0.790	−27.2	−1.8	0.06	−13.0	−0.1	1.00	FO
55865.719	0.799	−25.5	0.2	0.06	−12.9	−0.4	1.00	FO
55869.720	0.803	−27.8	−2.0	0.06	−11.9	0.5	1.00	FO

Note.
[a] KPNO = Kitt Peak National Observatory, FO = Fairborn Observatory.

(This table is available in its entirety in machine-readable form.)

T12; all 0.80 m aperture) with which each program star was discovered to be variable. From each T3 group sequence, three $V-C$ and two $K-C$ differential magnitudes are formed in each B and V passband and averaged together to create group means. Group mean differential magnitudes with internal standard deviations greater than 0.01 mag are discarded to eliminate observations taken under nonphotometric conditions. The surviving group means are corrected for extinction, transformed to the standard Johnson system and treated as single observations thereafter. Further information on the operation of the T3 APT and the reduction of the data can be found in Henry (1995a, 1995b) and Eaton et al. (2003).

All nine program star groups were observed up to five times each night at intervals of 2–3 hr throughout the duration of their observing seasons. In addition, each program group was observed continuously for several hours on one night near opposition. This observing strategy helped to minimize the inevitable 1 day aliases that appear in single-site data. The last two columns of Table 9 list the standard deviations of the final set of group mean $V-C$ and $K-C$ differential magnitudes in Johnson B. In each case, the standard deviations of the $K-C$ observations are near the limit of nightly precision for the T3 APT, while the standard deviations of the $V-C$ observations are always larger, confirming that the observed variability in each case is intrinsic to the program star. The difference is minimal for HD 210719, but see the discussion in Section 5.9. The individual observations of each star that passed the "cloud filtering" tests are listed in Table 10.

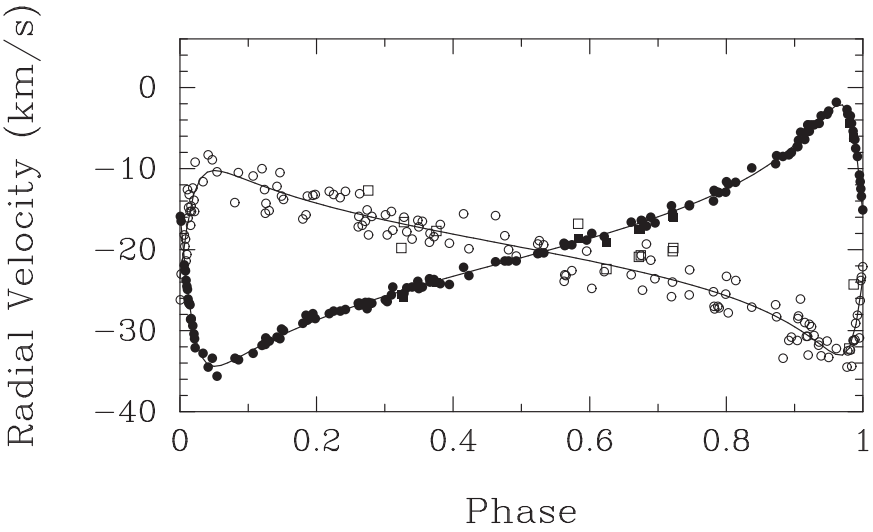

Figure 5. A plot of the radial velocities of the double-lined binary HD 182735 (Open symbols = primary and solid symbols = secondary) compared with the computed velocity curves (solid lines). Squares = KPNO and circles = Fairborn Observatory. Phase zero is a time of periastron passage. The binary has an orbital period of 1052.4 days and a high eccentricity of 0.728.

Table 8
HD 182735 Spectroscopic Orbital Elements and Related Parameters

Parameter	Value
P (days)	1052.38 ± 0.25
T (HJD)	$2{,}457{,}129.51 \pm 0.62$
e	0.7277 ± 0.0017
ω (deg)	260.26 ± 0.50
K_A (km s^{-1})	11.40 ± 0.28
K_B (km s^{-1})	16.158 ± 0.070
γ (km s^{-1})	-20.242 ± 0.041
$a_A \sin i$ (10^6 km)	113.19 ± 2.80
$a_B \sin i$ (10^6 km)	160.37 ± 0.82
$m_A \sin^3 i$ ($M_\odot$)	0.4318 ± 0.0095
$m_B \sin^3 i$ ($M_\odot$)	0.305 ± 0.013
Standard error of an observation of unit weight (km s^{-1})	0.5

Table 9
Program, Comparison, and Check Stars

APT	Program	Comparison	Check	$\sigma_{(V-C)}$[a] (mag)	$\sigma_{(K-C)}$[a] (mag)
T12	HD 6260	HD 6656	HD 5468	0.0073	0.0046
T12	HD 19649	HD 20813	HD 19648	0.0095	0.0044
T12	HD 28819	HD 29745	HD 31362	0.0060	0.0044
T12	HD 34415	HD 34316	HD 33336	0.0174	0.0041
T12	HD 58431	HD 59377	HD 60111	0.0084	0.0053
T12	HD 122928	HD 119784	HD 119288	0.0076	0.0053
T10	HD 144839	HD 145228	HD 145891	0.0316	0.0051
T10	HD 182735	HD 175987	HD 176408	0.0060	0.0043
T8	HD 210719	HD 209875	HD 210267	0.0043	0.0042

Note.
[a] In the Johnson B photometric band.

4.2. Analyses

As in our previous papers in this series, we used the method of Vaníček (1971), based on least-squares fitting of sinusoids, to search for periodicities in our photometric data sets of the nine γ Dor candidates. An important feature of this technique is its ability to uncover multiple frequencies in a single light curve. This is an iterative process in which each detected frequency, but not its associated amplitude, phase, or mean brightness level, is introduced as a fixed parameter into a new search for additional frequencies. The new search consists of simultaneously fitting a new mean brightness level along with the amplitudes and phases of all frequencies introduced as fixed parameters. In the resulting least-squares spectra, we plot the fractional reduction of the variance (reduction factor) versus trial frequency for each detected frequency.

For each program star, we analyzed the $V-C$ data sets separately in each photometric band over the frequency range 0.01–30.0 day^{-1}, which corresponds to the period range 0.033–100 days. The results of these analyses are given in Table 11. The $N_{\rm obs}$ given in column 4 is the number of observations surviving the cloud filter described above and the additional removal of obvious outliers. The frequencies and corresponding periods are given in columns 5 and 6. In every case, we find the same frequencies in both the B and V light curves. The peak-to-peak amplitudes reported in column 8 of the table are determined for each frequency *without* prewhitening for the other frequencies; column 9 shows that most of the B/V amplitude ratios are 1.15 or larger, eliminating the

Table 10
Individual Photometric Observations of 9 New γ Dor Stars

HD	Helio. Julian Date HJD–2,400,000	Var B (mag)	Var V (mag)	Chk B (mag)	Chk V (mag)
6260	54373.8511	0.553	0.613	−0.711	−0.456
6260	54373.9430	0.546	0.613	−0.720	99.999
6260	54377.6559	0.565	0.622	99.999	−0.468
6260	54377.7457	0.573	0.625	−0.717	−0.454
6260	54377.8381	0.575	0.621	99.999	−0.470
6260	54377.9272	0.568	0.623	−0.715	−0.460

Note. A "99.999" signifies that the differential magnitude was discarded because its internal standard deviation exceeded 0.01 mag.

(This table is available in its entirety in machine-readable form.)

Table 11
Photometric Results for Nine New γ Dor Stars

HD (1)	Photometric Band (2)	Date Range (HJD–2,400,000) (3)	N_{obs} (4)	Frequency (day^{-1}) (5)	Period (days) (6)	TESS (7)	Peak-to-peak Amplitude (mmag) (8)	B/V Amplitude Ratio (9)	T_{min} (HJD–2,400,000) (10)
6260	*B*	54,371.67–54,509.60	181	1.38803 ± 0.00032	0.72045 ± 0.00016	✓	11.3 ± 1.3	1.92 ± 0.32	54,430.454 ± 0.013
				1.46205 ± 0.00038	0.68397 ± 0.00018	✓	7.6 ± 1.4	0.99 ± 0.33	54,430.337 ± 0.021
	V	54,371.67–54,509.60	183	1.38800 ± 0.00034	0.72046 ± 0.00018	✓	5.9 ± 1.2		54,430.478 ± 0.023
				1.46350 ± 0.00032	0.68329 ± 0.00015	✓	7.7 ± 1.1		54,430.279 ± 0.016
19649	*B*	54,371.91–54,534.60	216	0.94354 ± 0.00028	1.05984 ± 0.00031	✓	18.3 ± 1.5	1.25 ± 0.17	54,450.729 ± 0.013
				0.89775 ± 0.00030	1.11390 ± 0.00037	✓	14.0 ± 1.5	1.24 ± 0.22	54,450.040 ± 0.022
				1.04214 ± 0.00029	0.95956 ± 0.00027	✓	11.9 ± 1.7	0.97 ± 0.26	54,450.591 ± 0.022
	V	54,373.81–54,534.60	195	0.94252 ± 0.00036	1.06099 ± 0.00041	✓	14.6 ± 1.3		54,450.740 ± 0.013
				0.89626 ± 0.00030	1.11575 ± 0.00037	✓	11.3 ± 1.3		54,450.105 ± 0.022
				1.04319 ± 0.00031	0.95860 ± 0.00028	✓	12.3 ± 1.4		54,450.601 ± 0.017
28819	*B*	54,372.02–54,562.62	237	3.51010 ± 0.00021	0.28489 ± 0.00002	✓	8.7 ± 0.9	1.50 ± 0.24	54,450.248 ± 0.005
	V	54,372.02–54,562.62	237	3.51156 ± 0.00018	0.28477 ± 0.00002	✓	5.8 ± 0.8		54,450.257 ± 0.007
34415A	*B*	54,371.87–54,561.63	322	0.94532 ± 0.00025	1.05784 ± 0.00028	✓	39.0 ± 1.7	1.27 ± 0.09	54,460.902 ± 0.007
				0.97627 ± 0.00029	1.02431 ± 0.00030	✓	30.0 ± 2.3	1.27 ± 0.15	54,460.564 ± 0.012
				0.88817 ± 0.00028	1.12591 ± 0.00035	X	14.7 ± 2.6	1.29 ± 0.36	54,460.548 ± 0.034
				0.91529 ± 0.00023	1.09255 ± 0.00027	X	16.0 ± 2.7	1.15 ± 0.32	54,460.293 ± 0.029
	V	54,371.87–54,560.63	326	0.94514 ± 0.00026	1.05804 ± 0.00029	✓	30.8 ± 1.3		54,460.906 ± 0.007
				0.97586 ± 0.00024	1.02474 ± 0.00025	✓	23.6 ± 1.8		54,460.556 ± 0.012
				0.88705 ± 0.00024	1.12733 ± 0.00030	X	11.4 ± 2.1		54,460.532 ± 0.034
				0.91420 ± 0.00026	1.09385 ± 0.00031	X	13.9 ± 2.1		54,460.316 ± 0.024
58431	*B*	54,373.01–54,586.63	267	2.33709 ± 0.00018	0.42788 ± 0.00003	✓	14.2 ± 1.2	1.42 ± 0.19	54,480.425 ± 0.006
				1.64711 ± 0.00018	0.60712 ± 0.00006	✓	10.9 ± 1.3	1.33 ± 0.25	54,480.003 ± 0.017
	V	54,373.97–54,586.63	265	2.33659 ± 0.00018	0.42797 ± 0.00003	✓	10.0 ± 1.1		54,480.409 ± 0.007
				1.64711 ± 0.00017	0.60712 ± 0.00006	✓	8.2 ± 1.1		54,480.028 ± 0.013
122928	*B*	54,073.04–54,282.75	325	2.57058 ± 0.00020	0.38902 ± 0.00003	—	11.4 ± 1.0	1.07 ± 0.17	54,200.254 ± 0.006
				2.36802 ± 0.00019	0.42229 ± 0.00003	—	9.1 ± 1.1	1.25 ± 0.26	54,200.211 ± 0.008
	V	54,072.04–54,286.66	312	2.57097 ± 0.00021	0.38896 ± 0.00003	—	10.7 ± 0.9		54,200.256 ± 0.005
				2.36797 ± 0.00019	0.42230 ± 0.00003	—	7.3 ± 1.0		54,200.199 ± 0.009
144839	*B*	54,544.85–54,640.74	201	2.20767 ± 0.00042	0.45297 ± 0.00009	—	65.3 ± 4.6	1.46 ± 0.15	54,590.240 ± 0.005
	V	54,544.85–54,640.74	201	2.20794 ± 0.00043	0.45291 ± 0.00009	—	44.8 ± 3.7		54,590.249 ± 0.006
182735A	*B*	54,371.69–54,648.94	293	2.07866 ± 0.00012	0.48108 ± 0.00003	✓	8.0 ± 0.9	1.40 ± 0.25	54,600.213 ± 0.009
	V	54,371.69–54,648.94	260	2.08323 ± 0.00012	0.48002 ± 0.00003	✓	5.7 ± 0.8		54,600.213 ± 0.010
210719	*B*	54,371.79–54,648.84	167	1.54237 ± 0.00015	0.64835 ± 0.00006	—	5.9 ± 0.9	0.94 ± 0.31	54,500.404 ± 0.015
	V	54,371.70–54,648.84	171	1.54228 ± 0.00018	0.64839 ± 0.00007	—	6.3 ± 1.0		54,500.411 ± 0.016

Note. The individual photometric observations are given in Table 10. Check marks in col. 8 indicate the frequencies/periods detected by TESS (✓ = detected, X = not detected, — = not observed).

ellipticity effect in a binary system ($B/V \approx 1.0$) or spot rotation of an active star ($B/V \approx 1.12$–1.14) as possible causes of brightness variability (Henry et al. 2000).

The resulting least-squares spectra and phase diagrams for the Johnson B observations of all nine program stars are shown below in the subsections for each individual star. Although all analyses were done over the full frequency range of 0.01–30.0 day^{-1}, the least-squares spectra are plotted over more restricted ranges; none of the stars exhibited variability in the frequency range 20–30 day^{-1}, and several showed no variability above 5 day^{-1}. The plots of the least-squares spectra show the results of successively fixing each detected frequency until no further frequencies could be found in both the B and V data sets. The frequency spectra all exhibit the presence of ± 1 day aliases, but our observing strategy described above resulted in reducing their power below that of the true signals. With all of the detected frequencies fixed, the rms of the residuals was usually close to the expected precision of the observations, indicating little or no remaining variability. To illustrate the low amplitudes, the phase diagrams are plotted for each frequency after the light curves were prewhitened to remove the other detected frequencies.

4.3. Criteria for Confirmation of γ Dor Variability

We use the following criteria for confirming our candidates to be γ Doradus variables: (1) late A to early F spectral class, (2) luminosity class V, IV–V, or IV, and (3) periodic photometric variability in the approximate range of 0.3–3 days that is attributable to pulsations. In Section 3.2.1, we described how our spectra acquired at KPNO and Fairborn allow the determination of the spectral and luminosity classes. In Section 4.2, we described the analysis of the T3 APT observations to determine the periodicities present in the photometry. We require that each period be detected in both the Johnson B and V passbands. The known γ Dor stars are generally multiperiodic, but we confirm monoperiodic variables if we can establish the likely presence of additional unresloved periods or if we can demonstrate that the variability must arise from pulsation. See Henry et al. (2007, 2011) for further details concerning the confirmation of γ Dor variables.

4.4. Comparison with TESS Photometry

As mentioned above in the description of our sample, all nine stars appear in the revised TIC (Stassun et al. 2019) prepared for the TESS mission (Ricker et al. 2015). To date, only six of the nine stars have been observed with TESS and, as yet, none have published results. We decided to perform preliminary period analyses on the available TESS data using the method of Vaníček (1971) to compare with our APT photometric results obtained in the same way. This would provide confirmation that the analysis of our single-site, ground-based photometry leads to the correct interpretation of the light curves. In addition, for cases where our ground-based results find only one frequency (period) with confidence, the TESS data may detect the presence of additional frequencies, helping to confirm the star as a γ Dor variable. We find that TESS confirms nearly all of the periods found in our photometry (see column 7 of Table 11). The TESS results for individual stars are given in Section 5 below.

5. Notes on Individual Stars

5.1. HD 6260 = HIP 5024

The star HD 6260 has previously aroused only slight interest. HD 6260 was one of more than 2500 stars in the Hipparcos catalog that Koen & Eyer (2002) identified as new candidate periodic variables. Their analysis of the Hipparcos photometry identified a frequency of 9.67007 day^{-1} in HD 6260, corresponding to a period of 0.1034 day, and an amplitude of just 0.008 mag.

The radial velocity of HD 6260 was measured as part of the complementary basic data program for stars with Hipparcos parallaxes. Duflot et al. (1992) obtained two objective prism velocities, 28 and -28 km s^{-1}, resulting in an average velocity of 0 km s^{-1}. Our three KPNO velocities produce a mean of 5.5 ± 0.8 km s^{-1}, while our 33 more recent Fairborn velocities have a similar average of 3.3 ± 0.2 km s^{-1}. The two Duflot et al. (1992) velocities that differ by 56 km s^{-1} were obtained five nights apart. While our KPNO and Fairborn observations show velocity variability, we find no evidence of the huge difference indicated by the two objective prism velocities and conclude that HD 6260 is a single star. We classify HD 6260 as an A9 dwarf and measure an average $v \sin i$ value of 51 km s^{-1}.

We obtained 218 group observations of HD 6260 with the T3 APT from 2007 September 27 through 2008 February 12 (Table 10). We were unable to get a good night of monitoring observations for this star. The results of our photometric analysis of these data are given in Table 11. We find two closely spaced frequencies at 1.38803 ± 0.00032 and 1.46205 ± 0.00038 day^{-1} in the Johnson B passband (Figure 6), corresponding to periods of 0.72045 and 0.68397 days. Both periods were also detected in the V data set. The peak-to-peak amplitudes in the B passband are 11.3 and 7.6 mmag, respectively. The light curve phased to each period is sinusoidal (Figure 7). The weighted mean of the two B/V amplitude ratios is 1.25 ± 0.22, consistent with pulsation. Our analysis of the TESS data finds several γ Dor periods, including the two found in our photometry.

Given a moderate number of radial velocities, which have a total range of 6.1 km s^{-1}, we searched for periods indicative of pulsation. In the velocity data we found no evidence of the two periods seen in the photometry. Instead, our 36 velocities (Table 2) show two possible low-amplitude pulsation periods, 0.46678 ± 0.00001 and 0.89477 ± 0.00001 days, which are in the γ Dor period range. As an example of the fit, in Figure 8 we compare the velocities phased with the 0.89477 day period with a sine curve. The fit has an amplitude of just 2.8 km s^{-1}. While we believe that this star is single, additional velocities will be required to determine whether either or both of the possible spectroscopic pulsational periods are real.

Based on these spectroscopic and photometric properties, we confirm HD 6260 as a new γ Dor variable.

5.2. HD 19649 = HIP 14696

HD 19649 was one of 62 objects that Drilling (1973) studied to determine the space distribution of stars later than A7 in two high galactic latitude regions. He acquired Johnson *UBV* photometry of HD 19649 and estimated an objective prism spectral class of F2:. Both Perry & Johnston (1982) and Olsen (1983) obtained Strömgren photometry of this star.

Nordström et al. (1997) determined velocities of nearly 600 early F dwarfs. For HD 19649, they computed an average

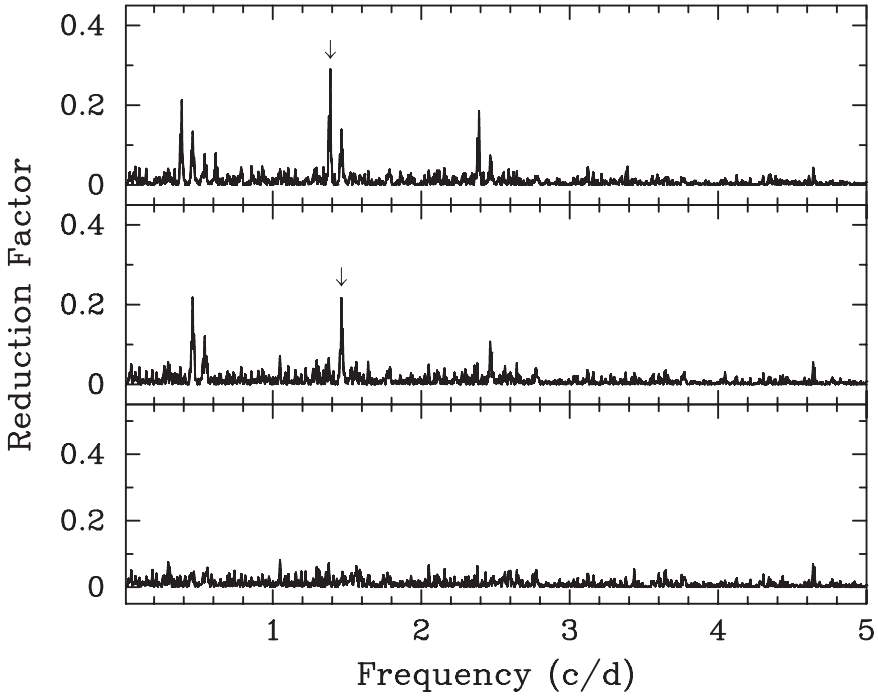

Figure 6. Least-squares frequency spectra of the HD 6260 Johnson *B* data set, showing the results of progressively fixing the two detected frequencies. The arrows indicate the two frequencies at 1.38803 day^{-1} (top) and 1.46205 day^{-1} (middle). The bottom panel shows the frequency spectrum with these two frequencies fixed. Both frequencies were confirmed in the Johnson *V* data set.

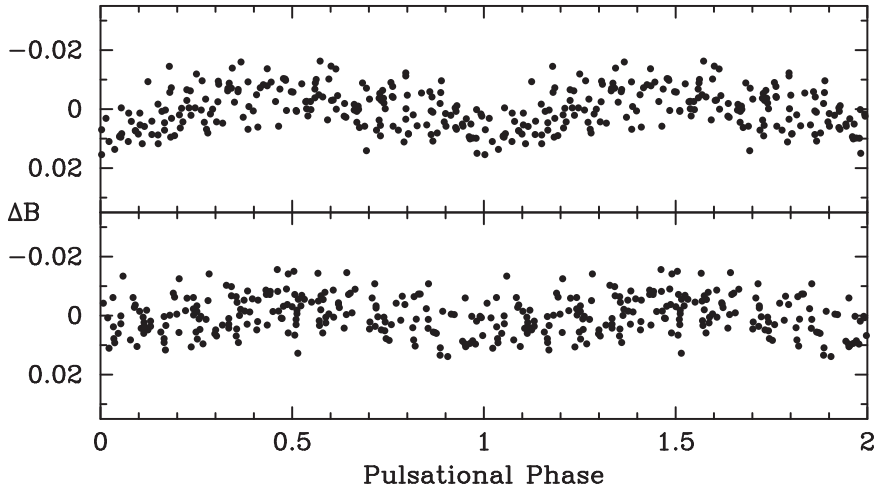

Figure 7. The Johnson *B* photometric data for HD 6260, phased with the two frequencies and times of minimum from Table 11. The two frequencies are 1.38803 day^{-1} (top) and 1.46205 day^{-1} (bottom). For each panel, the data set has been prewhitened to remove the other known frequency.

velocity of 14.2 ± 1.0 km s^{-1} from three observations. From three 80 Å mm^{-1} spectra, Grenier et al. (1999) found a similar average velocity of 14.0 ± 2.1 km s^{-1}. Our three KPNO velocities result in an average of 13.1 ± 0.6 km s^{-1}, while our eight Fairborn velocities have an average of 12.9 ± 0.5 km s^{-1}. The averages from the four data sets are consistent, and so the star appears to be single.

In addition to the spectral class of F2: by Drilling (1973), Grenier et al. (1999) classified HD 19649 as F2 IV. We find the star to be an F2 subgiant in good agreement with the previous results. Nordström et al. (1997) estimated a projected rotational velocity of 45.9 km s^{-1}. Our average value of 44 km s^{-1} is in accord with that result.

We obtained 253 group observations of HD 19649 with the T3 APT between 2007 September 27 and 2008 March 8 (Table 10). The results of our photometric analysis are given in Table 11. We find three frequencies at 0.94354 ± 0.00028, 0.89775 ± 0.00030, and 1.04214 ± 0.00029 day^{-1} in the Johnson *B* passband (Figure 9), corresponding to periods of 1.05984, 1.11390, and 0.95956 days. All three periods were confirmed in the *V* data set. The peak-to-peak amplitudes in the *B* passband are 18.3, 14.0, and 11.9 mmag. The light curve is sinusoidal when phased with each of the three periods (Figure 10). The weighted mean of the three B/V amplitude ratios is 1.19 ± 0.12, consistent with pulsation. We find the same three periods in the TESS data, along with several others.

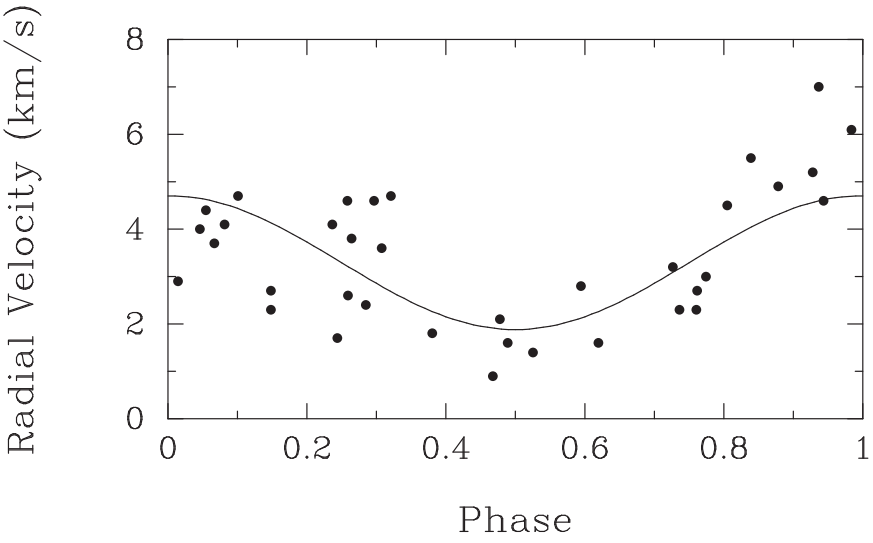

Figure 8. Radial velocities of HD 6260 phased with a period of 0.89477 day. The time of maximum velocity is HJD 2456933.72 ± 0.03 and the amplitude of the sine curve fit is 2.8 ± 0.3 km s^{-1}.

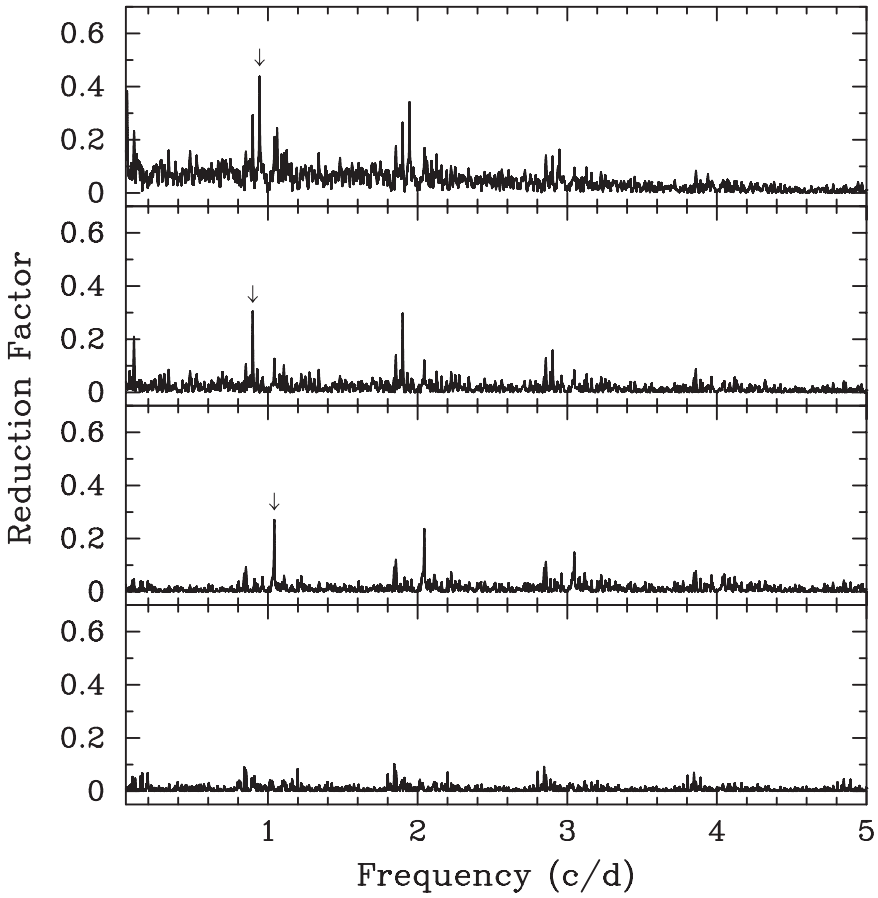

Figure 9. Least-squares frequency spectra of HD 19649 in Johnson *B*, showing the results of progressively fixing the three detected frequencies. The arrows indicate the three frequencies (top to bottom): 0.94354, 0.89775, and 1.04214 day^{-1}. All three frequencies were confirmed in the Johnson *V* data set.

Based on these properties, we confirm HD 19649 to be a new γ Dor variable.

5.3. HD 28819 = HIP 21246

HD 28819 is a star that is situated in front of the nearby Taurus–Auriga molecular cloud, a complex region of recent star formation that contains dozens of T Tauri stars (e.g., Moneti et al. 1984). Perry & Johnston (1982) and Olsen (1983) obtained Strömgren photometry of it as part of their extensive general photometric surveys. Because HD 28819 is in the foreground field of the cloud, it has been included in several studies of the stars in the cloud complex. Slutskij et al. (1980) made Johnson *UBVRI* observations of the star. Feigelson & Kriss (1983) observed HD 28819 as part of a spectroscopic

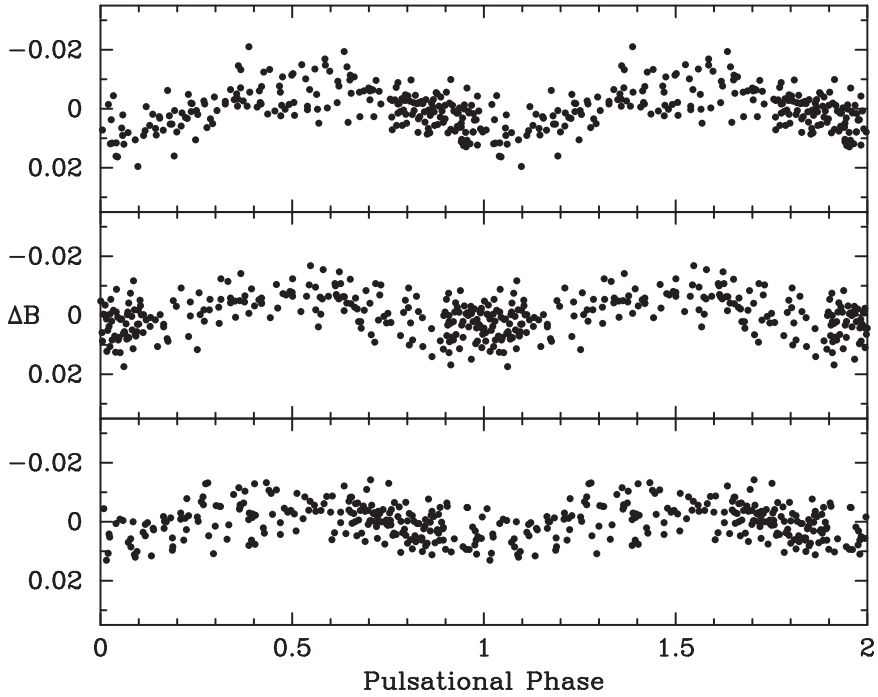

Figure 10. The Johnson *B* photometric data for HD 19649, phased with the three frequencies and times of minimum from Table 11. The three frequencies are (top to bottom) 0.94354, 0.89775, and 1.04214 day^{-1}. For each panel, the data set has been prewhitened to remove the other known frequencies.

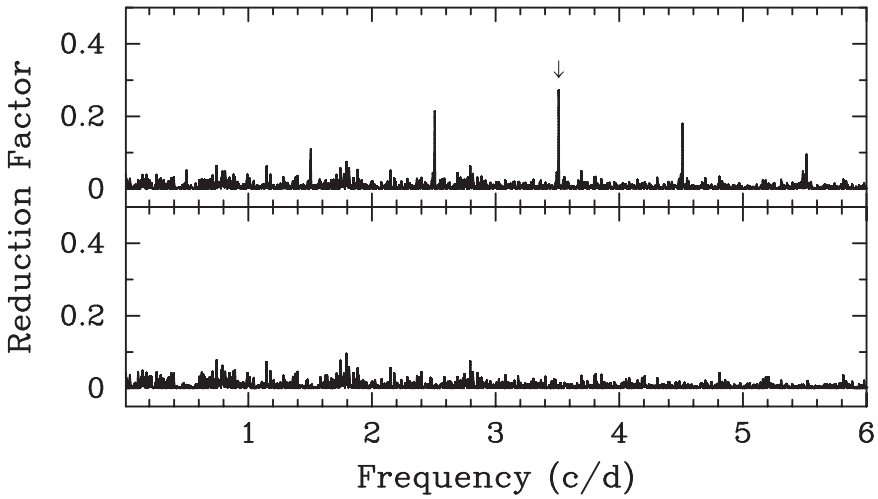

Figure 11. Least-squares frequency spectra of the HD 28819 Johnson *B* data set. The arrow in the top panel indicates the single detected frequency of 3.51010 day^{-1}. The bottom panel is the frequency spectrum resulting when the 3.51010 day^{-1} frequency is fixed. The same frequency was found in the Johnson *V* data set.

survey to identify pre-main-sequence stars with weak Hα emission. They classified it as an A8 star and determined that it has normal Hα absorption for its spectral class. Moneti et al. (1984) obtained optical polarimetry of HD 28819, while Jensen et al. (2004) collected infrared polarimetry. Kenyon et al. (1994) acquired spectrophotometry of it as part of a study to determine the extinction law for the cloud.

HD 28819 was included in a complementary project for stars with Hipparcos parallaxes. Grenier et al. (1999) obtained three low-dispersion radial velocities of HD 28819 with an average of 26.1 ± 2.8 km s^{-1} and determined a spectral classification of F0 V. Our KPNO average velocity from two spectra is 27.0 ± 0.2 km s^{-1}, while the result from the 11 more recent Fairborn velocities is 24.1 ± 0.6 km s^{-1}. In agreement with Grenier et al. (1999), we find a spectral class for HD 28819 of F0 and a dwarf luminosity class. Our average projected rotational velocity is 110 km s^{-1}. The velocity variations are modest, and there is no significant evidence of orbital motion. Thus, we consider the star to be single.

We obtained 251 group observations of HD 28819 with the T3 APT between 2007 September 28 and 2008 April 6 (Table 10). The results of our photometric analysis are given in Table 11. We find one frequency in the Johnson *B* passband at 3.51010 ± 0.00021 day^{-1} (Figure 11), corresponding to a period of 0.28489 day. The light curve is sinusoidal with an amplitude of 8.7 mmag (Figure 12). The same period is found in the *V* data set. The B/V amplitude ratio is 1.50 ± 0.24, consistent with pulsation. Our analysis of the TESS data finds the same period along with several others in the γ Dor period range.

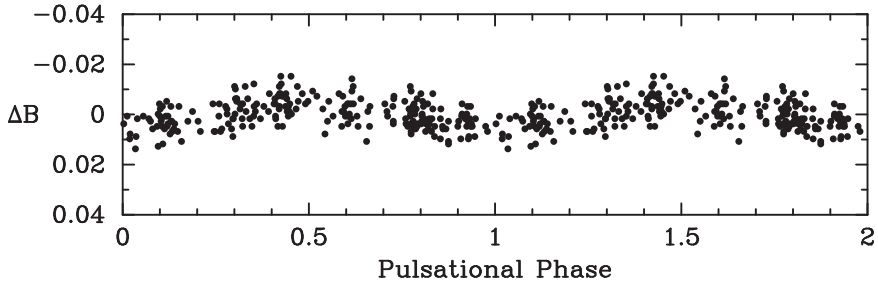

Figure 12. The Johnson *B* photometric data for HD 28819, phased with the 3.51010 day^{-1} frequency and time of minimum from Table 11.

The 0.28489 day period of HD 28819 falls at the short end of the observed 0.3 to 2.6 days range of periods in the list of 86 known γ Dor field stars in Henry et al. (2011, Table 8). We computed HD 28819's pulsation constant as defined by Handler & Shobbrook (2002) and find $\log Q = -0.76$, while $\log P = -0.54$. Both of these values fall within the short-period tails of the Q and P distributions for γ Dor stars (Handler & Shobbrook 2002, Figure 9). The location of HD 28819 in the H-R diagram falls in the overlap region of the δ Sct and γ Dor instability strips where several hybrid pulsators are located. Our photometry indicates possible high-frequency variability around 23 day^{-1}, but this is not confirmed in both passbands.

Given these spectroscopic and photometric properties, we classify HD 28819 as a new γ Dor variable.

5.4. HD 34415 = HIP 24693

Knude (1977) included HD 34415 in an extensive Strömgren photometry survey of 750 A and F stars. Those observations were used to estimate distances and interstellar reddening. HD 34415 was also part of the Strömgren photometry surveys of Perry & Johnston (1982) and Olsen (1983). Nordström et al. (1997) included HD 34415 in a sample of nearly 600 early F stars, analyzed to identify duplicity and measure rotational velocities. Their three velocities produced an average of 35.1 ± 0.6 km s^{-1}. They also estimated a $v \sin i$ value of 41.4 km s^{-1}.

Our spectra show that HD 34415 is a composite spectrum star consisting of a broad-lined star and a narrow-lined star with the lines of the latter being situated approximately in the center of the broader features (Figure 1). As discussed previously, from our velocities of both components that cover 12.5 yr plus three earlier velocities of the primary from Nordström et al. (1997), we have determined a preliminary spectroscopic orbit for both components that has a period of 6400 days (17.5 yr).

Recently, Kervella et al. (2019) determined the long-term proper motion of stars that are in both the Hipparcos and Gaia second data release catalogs. From those results they computed the long-term proper motion vector and compared it with the proper motion of the same star in either the Hipparcos or Gaia catalog to determine whether there is a significant difference that would indicate that the star is a long-period binary. They concluded from their astrometric analysis that HD 34415 is a binary, a result that we confirm from our radial velocity study.

Additional properties of the two components are a bit inconsistent. The $B - V$ value given in SIMBAD from the results of Hog et al. (2000) for the combined components suggests an average F3 V spectral type (Gray 1992), while the Strömgren $b - y$ and especially the Hβ value (Hauck & Mermilliod 1998) correspond to a spectral type that is 1–2 subclasses earlier (Crawford 1975). We classify components A and B as F0: dwarf and G2: dwarf, respectively, and from our spectrum addition fits, estimate a ΔV of 2.7 mag, which is somewhat larger than the canonical magnitude difference between the two spectral types. It is possible that motion of the unresolved binary has affected the parallax measurement and/or there is some reddening. Consistency would be improved if the system were more distant and the primary more evolved. The $v \sin i$ values of A and B are 41 and 5: km s^{-1}, respectively. The colon after some of the properties of the much fainter secondary indicates greater than usual uncertainty. Colors for the individual components have been adopted from our spectral types and the relation in Gray (1992).

We obtained 380 observations of HD 34415 with the T3 APT from 2007 September 27 through 2008 April 8 (Table 10). The results of our photometric analysis of these data are given in Table 11. We find four closely spaced frequencies at 0.94532 ± 0.00025, 0.97627 ± 0.00029, 0.88817 ± 0.00028, and 0.91529 ± 0.00023 day^{-1} in the Johnson *B* passband (Figure 13), corresponding to periods of 1.05784, 1.02431, 1.12591, and 1.09255 days. All four periods are also detected in the *V* observations. The peak-to-peak amplitudes in the *B* passband are 39.0, 30.0, 14.7, and 16.0 mmag, respectively. The light curve is sinusoidal when phased to each of these four periods (Figure 14). The weighted mean of the four B/V amplitude ratios is 1.26 ± 0.07, consistent with pulsation. We find the first two periods in the TESS data but not the other two, perhaps because their amplitudes are only half the first two periods.

Based on these spectroscopic and photometric properties, we confirm that the F0 component of HD 34415 is a new γ Dor variable.

5.5. HD 58431 = HIP 36059

As with many of the other stars in this paper, Olsen (1983) obtained Strömgren indices of HD 58431. HD 58431 was observed as part of the Nainital–Cape Survey, a search for photometric variability in northern hemisphere, chemically peculiar A stars (Joshi et al. 2006). Observations over 2.5 hr on two consecutive nights resulted in no evidence for light variability.

Using a probabilistic neural network model to classify spectra in the ELODIE stellar spectral library, Mahdi (2008) found HD 58431 to be an F0 V star. Our classification of F1 dwarf is in good agreement. With another neural network model, Giridhar et al. (2013) determined HD 58431 to be slightly iron poor compared to the Sun. Gontcharov (2006) lists a radial velocity of 7.4 ± 0.9 km s^{-1}. Our three KPNO velocities result in an average of 10.2 ± 0.03 km s^{-1}. The ten

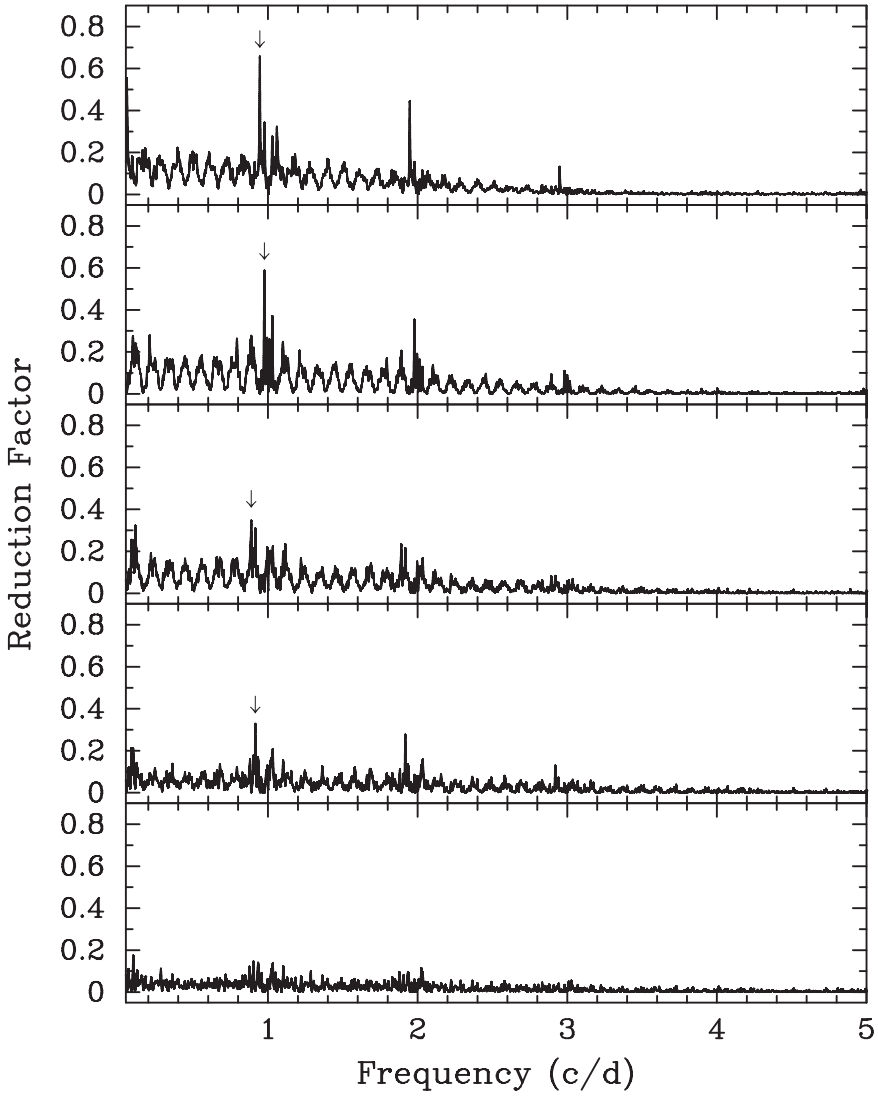

Figure 13. Least-squares frequency spectra of the HD 34415 Johnson *B* data set, showing the results of progressively fixing the four detected frequencies. The arrows indicate the four frequencies (top to bottom) 0.94532, 0.97627, 0.88817, and 0.91529 day^{-1}. All four frequencies were confirmed in the Johnson *V* data set.

Fairborn observations produce a similar value of 9.9 ± 0.2 km s^{-1}. From these results we conclude that HD 58431 is a single star. HD 58431 has the lowest $v \sin i$ value of the γ Dor pulsators in our study, 34 km s^{-1}.

We obtained 315 group observations of HD 58431 with the T3 APT from 2007 September 27 through 2008 April 29 (Table 10). The results of our photometric analysis are given in Table 11. We find two independent frequencies at 2.33709 ± 0.00018 and 1.64711 ± 0.00018 day^{-1} in the Johnson *B* passband (Figure 15), corresponding to periods of 0.42788 and 0.60712 days. Both periods were also detected in the *V* passband. The peak-to-peak amplitudes in *B* are 14.2 and 10.9 mmag, respectively. The light curves phased to each period are sinusoidal (Figure 16). The weighted mean of the two B/V amplitude ratios is 1.38 ± 0.15, consistent with pulsation. Both periods are found in the TESS data, along with two additional, comparatively weak periods also in the γ Dor period range.

Therefore, based on these properties, we confirm HD 58431 as a new γ Dor variable.

5.6. HD 122928 = HIP 68780

As with our other program stars, Perry & Johnston (1982) and Olsen (1983) obtained Strömgren photometry of HD 122928. The star also was included in the extensive spectroscopic study of Grenier et al. (1999). From three low-dispersion spectra, they determined an average radial velocity of -27.2 ± 3.9 km s^{-1}. They also estimated a spectral type of F0 IV. Our six KPNO velocities have an average of -22.7 ± 0.6 km s^{-1}, a value that is in good agreement with our average Fairborn velocity of -23.3 ± 0.2 km s^{-1}, which was determined from 22 spectra. Our KPNO and Fairborn average velocities differ by 4.5 km s^{-1} or less from that of Grenier et al. (1999), similar to the uncertainty in their average, and so we conclude that the results to date provide no strong evidence that the star is a binary. Therefore, we assume that the star is single. Our spectral type of F0 dwarf is similar to that of Grenier et al. (1999). We find a $v \sin i$ value of 69 km s^{-1}.

We obtained 373 group observations of HD 122928 with the T3 APT between 2006 December 1 and 2007 July 4 (Table 10). The results of our photometric analysis are given in Table 11.

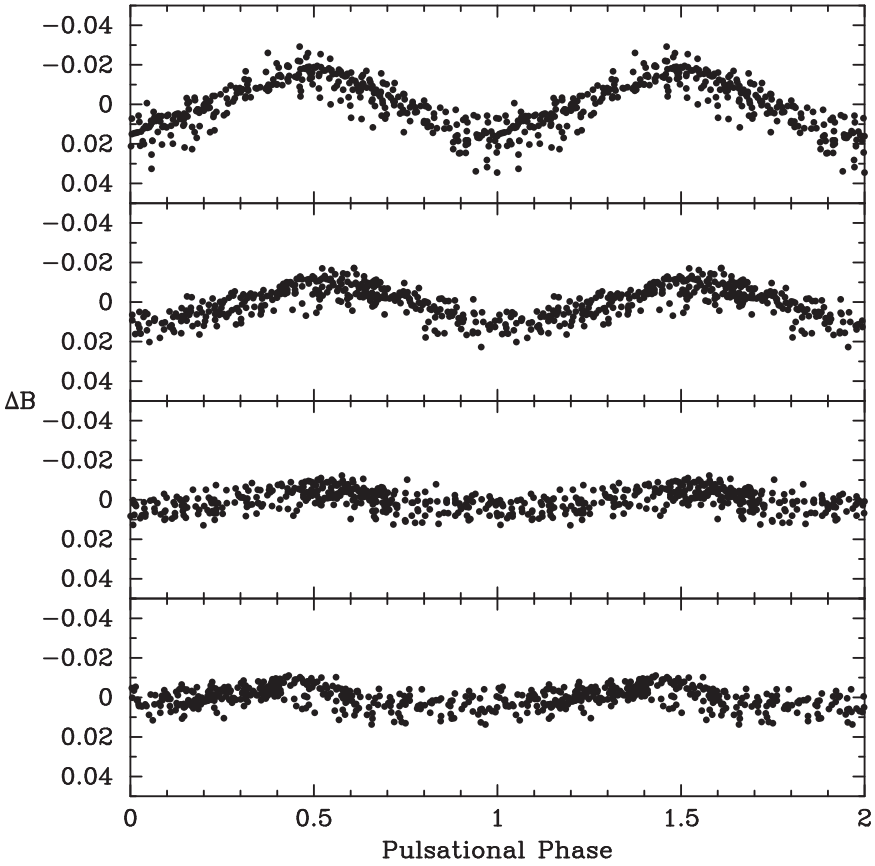

Figure 14. The Johnson *B* photometric data for HD 34415, phased with the four frequencies and times of minimum from Table 11. The four frequencies are (top to bottom) 0.94532, 0.97627, 0.88817, and 0.91529 day^{-1}. For each panel, the data set has been prewhitened to remove the other known frequencies.

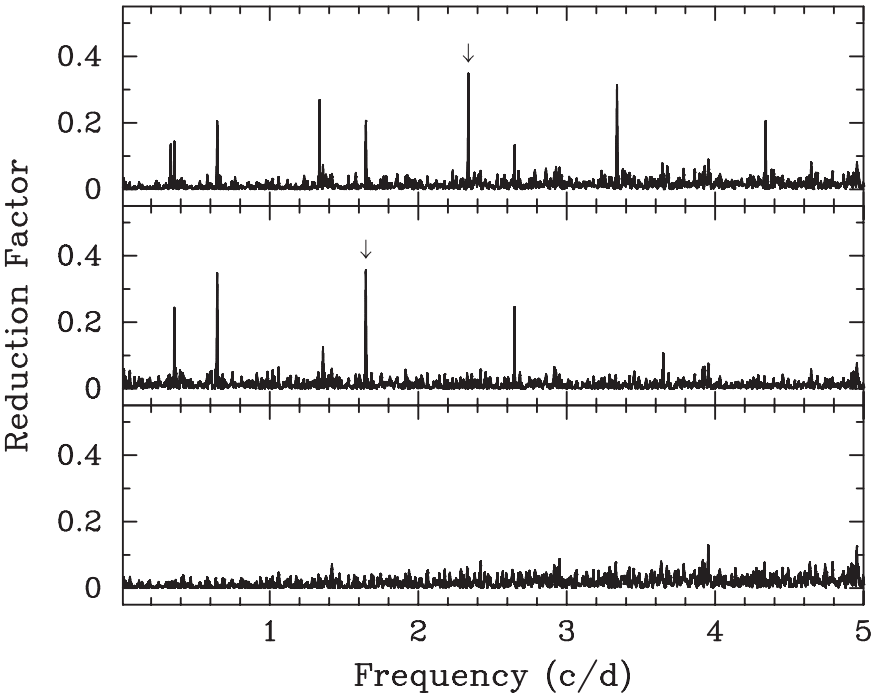

Figure 15. Least-squares frequency spectra of the HD 58431 Johnson *B* data set, showing the results of progressively fixing the two detected frequencies. The arrows indicate the two frequencies at 2.33709 day^{-1} (top) and 1.64711 day^{-1} (middle). Both frequencies were confirmed in the Johnson *V* data set.

We find two frequencies at 2.57058 ± 0.00020 and 2.36802 ± 0.00019 day^{-1} in the Johnson *B* passband (Figure 17), corresponding to periods of 0.38902 and 0.42229 days. Both periods are present in the *V* data set as well. The peak-to-peak amplitudes in the *B* passband are 11.4 and 9.1 mmag. The light curve is sinusoidal when phased with each of the periods

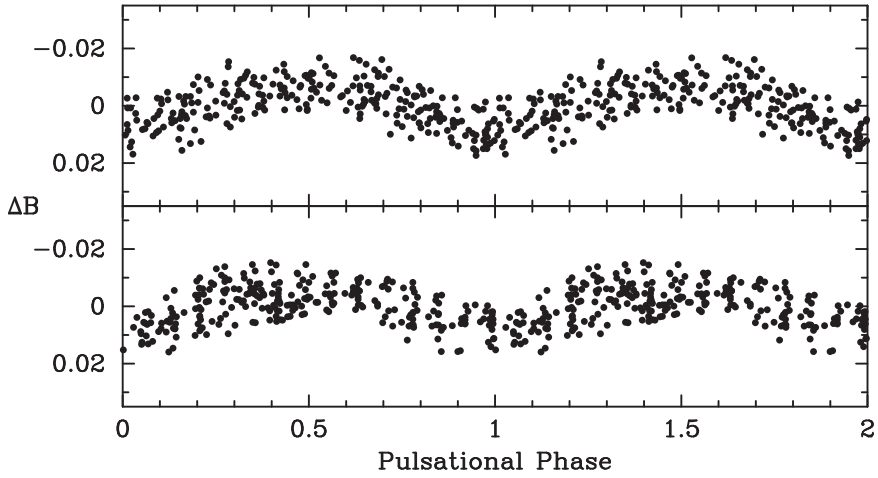

Figure 16. The Johnson *B* photometric data for HD 58431, phased with the two frequencies and times of minimum from Table 11. The two frequencies are 2.33709 day^{-1} (top) and 1.64711 day^{-1} (bottom). For each panel, the data set has been prewhitened to remove the other frequency.

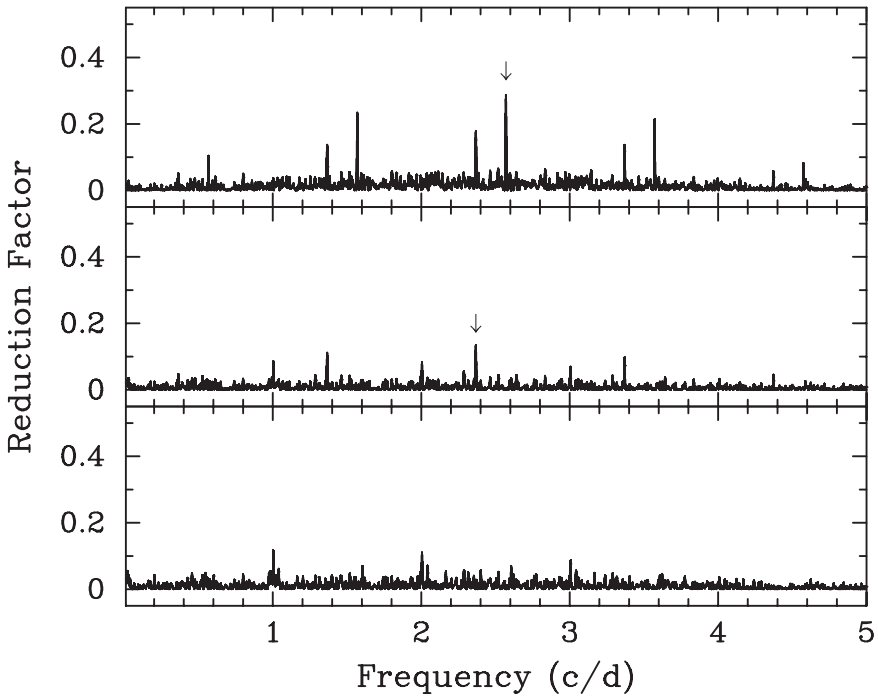

Figure 17. Least-squares frequency spectra of the HD 122928 Johnson *B* data set, showing the results of progressively fixing the two detected frequencies. The arrows indicate the two frequencies at 2.57058 day^{-1} (top) and 2.36802 day^{-1} (middle). Both frequencies were confirmed in the Johnson *V* data set.

(Figure 18). The weighted mean of the two B/V amplitude ratios is 1.12 ± 0.14, which is consistent with pulsation. There are no observations of HD 122928 from TESS but, given its spectroscopic and photometric properties described here, we can still confirm HD 122928 to be a new γ Dor variable.

5.7. HD 144839 = HIP 78993

HD 144839 was one of 374 stars with radial velocities obtained at the David Dunlap Observatory that were reported by Young (1942). From seven 66 Å mm^{-1} spectra, Young found an average radial velocity of -30.0 ± 7.0 km s^{-1}. He classified the spectrum as F2n, the "n" indicating nebulous, or broad, lines. The individual velocity measurements show a range of 33 km s^{-1}, which he suggested was larger than expected for such a broad-lined star but did not conclude that it was a binary. Harlan (1969) classified HD 144839 as an F3 III. More recently, HD 144839 was part of the extensive Strömgren photometric surveys of Olsen (1983, 1984).

We classify HD 144839 as an F0 dwarf with broad lines that have a rather large projected rotational velocity of 100 km s^{-1}. From their astrometric analysis of its proper motion anomaly, Kervella et al. (2019) determined that it is a long-period spectroscopic binary. Despite the very broad, shallow lines of this star, which significantly degrade our measured velocity precision, as discussed earlier, we have obtained a spectroscopic orbit for it that has a period of 995 days, confirming the conclusion of Kervella et al. (2019).

We obtained 239 group observations of HD 144839 with the T3 APT between 2008 March 18 and 2008 June 22 (Table 10). The results of our photometric analysis are given in Table 11. We find only one frequency in the Johnson *B* passband at 2.20767 ± 0.00042 day^{-1} (Figure 19), corresponding to a

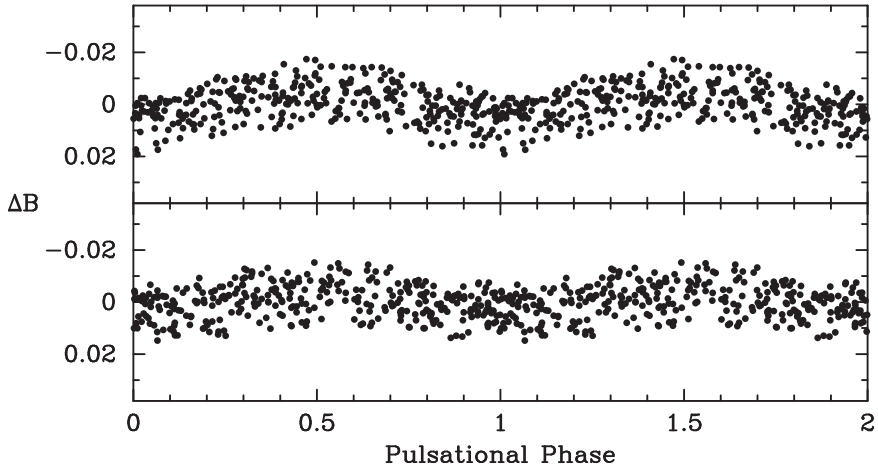

Figure 18. The Johnson *B* photometric data for HD 122928, phased with the two frequencies and times of minimum from Table 11. The two frequencies are 2.57058 day^{-1} (top) and 2.36802 day^{-1} (bottom). For each panel, the data set has been prewhitened to remove the other frequency.

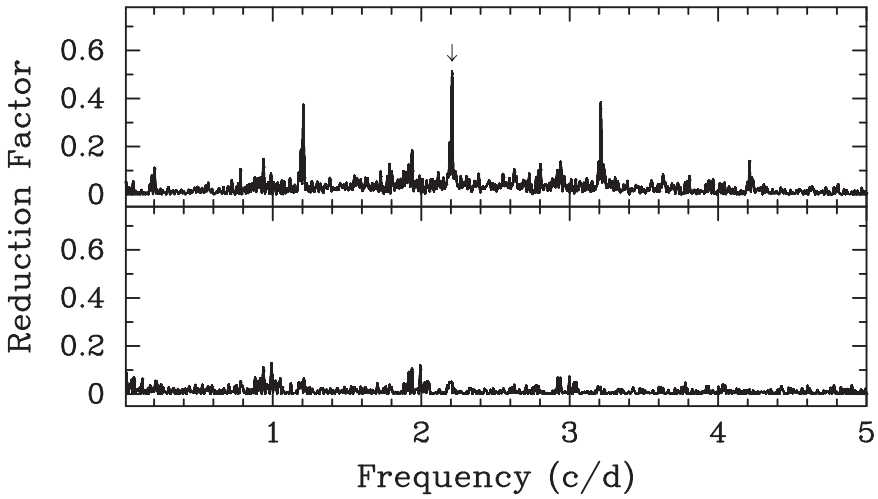

Figure 19. Least-squares frequency spectra of the HD 144839 Johnson *B* data set. The arrow in the top panel indicates the single detected frequency of 2.20767 day^{-1}. The bottom panel is the frequency spectrum resulting when the 2.20767 day^{-1} frequency is fixed. The same frequency was found in the Johnson *V* data set.

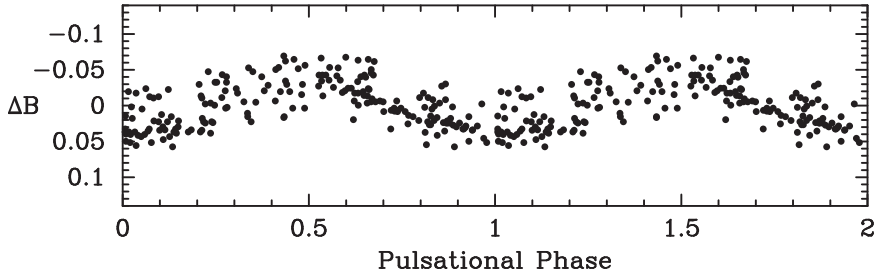

Figure 20. The Johnson *B* photometric data for HD 144839, phased with the 2.20767 day^{-1} frequency and time of minimum from Table 11.

period of 0.45297 day. We find the same period in the *V* data set. The light curve is sinusoidal with an amplitude of 65.3 mmag (Figure 20). The B/V amplitude ratio for the single period is 1.46 ± 0.15, consistent with pulsation. We have no data available from TESS.

In the course of analyzing the HD 144839 photometic data, we realized we had overlooked the existence of a close optical companion several magnitudes fainter and approximately 28″ away from HD 144839. This placed the companion on the very edge of the 55″ diaphragm we used to measure HD 144839 and its comp stars, resulting in considerable scatter in our $V - C$ differential magnitudes. Fortunately, the 65 mmag amplitude in HD 144839 is, by far, the largest photometric amplitude in our sample (Table 11), so its 0.45297 day period was still easily detected. The rms of the residuals to the least-squares sine fit was 0.021 mag, several times larger than the normal 0.003–0.005 mag rms for the other stars in this paper. A weaker period or two are likely to be present in the bottom panel of Figure 19, but we are unable to make any unique identifications in both the *B* and *V* passbands.

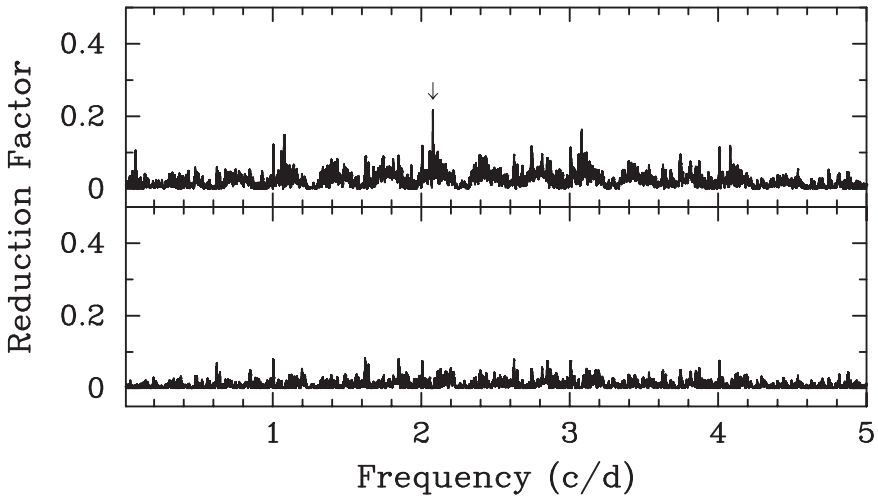

Figure 21. Least-squares frequency spectra of the HD 182735 Johnson *B* data set. The arrow in the top panel indicates the single detected frequency of 2.07866 day^{-1}. The bottom panel is the frequency spectrum resulting when the 2.07866 day^{-1} frequency is fixed. The same frequency was found in the Johnson *V* data set.

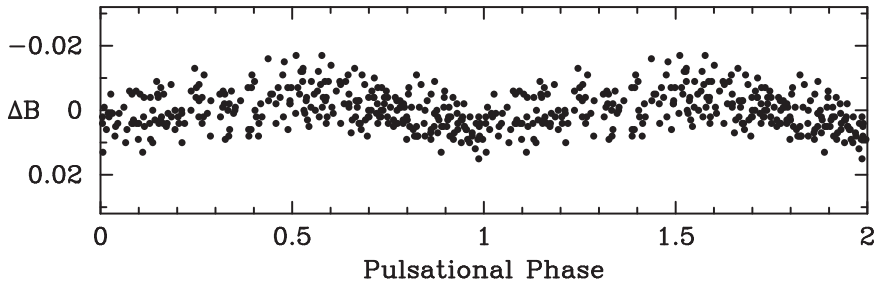

Figure 22. The Johnson *B* photometric data for HD 182735, phased with the 2.07866 day^{-1} frequency and time of minimum from Table 11.

Given the photometric and spectroscopic properties discussed here, we confirm HD 144839 to be a new γ Dor variable.

5.8. HD 182735 = HIP 95271

HD 182735 is yet another star for which Olsen (1983) acquired Strömgren photometry. Duflot et al. (1990) obtained five radial velocities from objective prism plates and found an average velocity of -26.0 ± 2.8 km s^{-1}. From three spectra, Nordström et al. (1997) measured an average radial velocity of -20.02 ± 4.56 km s^{-1} and determined a $v \sin i$ value of 23.8 km s^{-1}. They concluded from their large velocity range that HD 182735 has a variable velocity.

Makarov & Kaplan (2005) listed it as a potential binary based on the acceleration of its proper motion, but it was not flagged as such by Frankowski et al. (2007), who used slightly different criteria for their list of potential astrometric binaries. Recently, Kervella et al. (2019) confirmed that it has a proper motion anomaly and so is a long-period binary.

Our spectra show that HD 182735 has a composite spectrum consisting of a broad-lined star and a narrow-lined star (Figure 2). As discussed previously, we have determined spectroscopic orbital elements for this double-lined binary. The system has a period of 1052.4 days and a high eccentricity of 0.73.

We classify the primary and secondary as F1 dwarf and G2: dwarf, respectively. Component A is very broad lined with a $v \sin i$ value of 125 km s^{-1}, while component B has very narrow lines, resulting in $v \sin i$ of just 3: km s^{-1}. From our spectrum addition fits, we estimate $\Delta V = 2.2$ mag and adopt for the two components the colors from Gray (1992) for the above spectral types.

We obtained 313 group observations of HD 182735 with the T3 APT between 2007 September 27 and 2008 June 30 (Table 10). The results of our photometric analysis are given in Table 11. We find only one frequency at 2.07866 ± 0.00012 day^{-1} in the Johnson *B* band (Figure 21), corresponding to a period of 0.48108 day. The same period occurs in the *V* data set. The light curve is sinusoidal with an amplitude of 8.0 mmag (Figure 22). The B/V amplitude ratio for the single period is 1.40 ± 0.25, consistent with pulsation. The bottom panel of Figure 21 suggests the presence of additional weak frequencies in the γ Dor range, but we could not confirm the same frequencies in our *V* data. However, we find the 0.48 day period in the TESS data along with several others of low amplitude.

Therefore, we can confirm component A of HD 182735 as a new γ Dor variable.

5.9. HD 210719 = HIP 109614

As part of the Geneva-Copenhagen survey of the solar neighborhood, Olsen (1983, 1984) obtained Strömgren photometry of HD 210719. Nordström et al. (1997) determined a mean radial velocity of 20.64 ± 3.93 km s^{-1} from three measurements and estimated a $v \sin i$ value of 104 km s^{-1}. Our three KPNO velocities have an average of 24.5 ± 1.5 km s^{-1}, while our 48 Fairborn velocities have a mean of 18.3 ± 0.4 km s^{-1}. The result of Nordström et al. (1997) falls between our two averages, while our $v \sin i$ value of 111 km s^{-1} is just slightly greater than that of Nordström et al. (1997). We classify the star as an A9 dwarf.

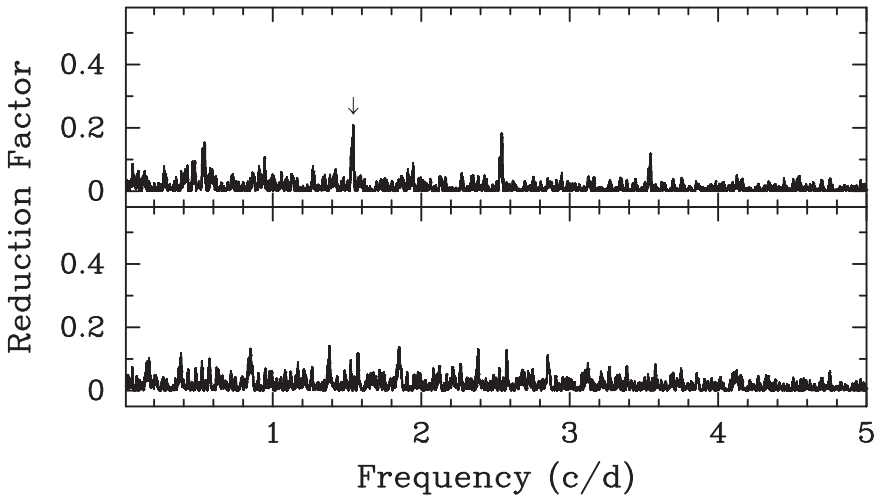

Figure 23. Least-squares frequency spectra of the HD 210719 Johnson *B* data set. The arrow in the top panel indicates the single detected frequency of 1.54237 day^{-1}. The bottom panel is the frequency spectrum resulting when the 1.54237 day^{-1} frequency is fixed. The same frequency was found in the Johnson *V* data set.

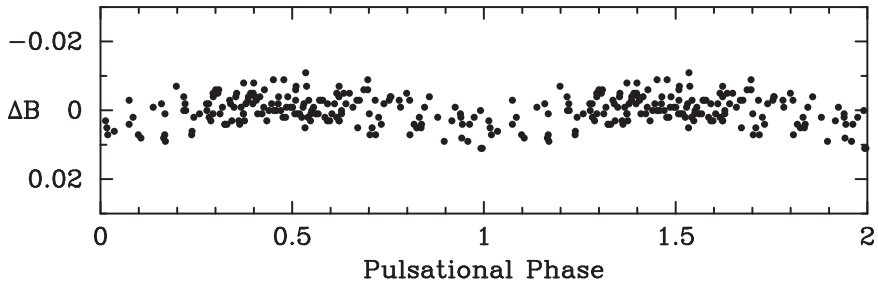

Figure 24. The Johnson *B* photometric data for HD 210719, phased with the 1.54237 day^{-1} frequency and time of minimum from Table 11.

Although the rapid rotation and line asymmetries of HD 210719 make velocity measurements less precise than in many of our other stars, the velocities certainly show real variability. Thus, we examined our velocities but did not find either the photometric period identified below or any other clear periodicities in the γ Dor period range. Extending the period search to 100 days also did not result in the identification of any periodic variability in the velocities. We conclude that HD 210719 is single with the observed velocity variations coming not from orbital motion but from pulsation.

We obtained 185 group observations of HD 210719 with T3 between 2007 September 27 and 2008 June 30 (Table 10). The results of our photometric analysis are given in Table 11. We find only one frequency in HD 210719 at 1.54237 ± 0.00015 day^{-1} in the Johnson *B* band (Figure 23), corresponding to a period of 0.64835 day. We find the same period in the *V* data set. The light curve is sinusoidal with an amplitude of only 5.9 mmag (Figure 24). Although the B/V amplitude ratio of 0.94 ± 0.33 is consistent with the ellipticity effect in a binary, its large error also encompases pulsation. We noted in Section 4.1 that the difference between the standard deviation of the $V-C$ and $K-C$ differential magnitudes was minimal (see Table 9). Our analysis of the $K-C$ observations was free of any periodicity. The bottom panel of Figure 23 suggests additional frequencies in the γ Dor range, but we could not match them up to similar low-amplitude frequencies in the *V* data. Unfortunately, HD 210719 has not been observed with TESS.

Given the star's early spectral class, the lack of evidence for a secondary component, the presence of radial velocity variations due to pulsations, and the evidence for additional photometric periods, we confirm HD 210719 as a new γ Dor variable.

6. Discussion

With the use of the *V* magnitudes, $B-V$ color indices, and parallaxes listed in Table 12, the nine new γ Dor variables discovered in this paper are plotted as filled circles in the H-R diagram of Figure 25. The magnitudes and color indices in columns 2 and 3 originate from the Tycho-2 catalog and are converted to the Johnson *UBV* photometric system with the equations derived by Hog et al. (2000). The parallaxes in column 4 come from the Gaia DR2 catalog (Gaia Collaboration et al. 2018). The absolute magnitudes in column 5 are derived from the *V* magnitudes and the parallaxes. All nine new γ Dor stars fall well within the observed γ Dor instability strip, which straddles the lower, red edge of the δ Sct instability strip (e.g., Henry et al. 2011; Ibanoglu et al. 2018).

Besides the nine new γ Dor stars discovered here, we include 64 additional γ Dor stars in Table 12 and Figure 25 that were discovered or confirmed in our APT program. Original references to these discoveries can be found in Henry et al. (2011). Our goal here is to examine the incidence of hybrid δ Sct/γ Dor variability in the overlap region of the two instability strips and compare our ground-based incidence rate with the detection of hybrid pulsators discovered in recent space-based observations.

We limit our ground-based search to the 73 γ Dor stars from our APT program because they were uniformly observed with our T3 0.40 m APT following the procedures described in

Table 12
γ Dor Stars Discovered or Confirmed by APT Program

HD[a]	V[b] (mag)	$(B-V)$[b,c] (mag)	π[d] (mas)	M_V[e] (mag)	Duplicity[f]	HR Region
(1)	(2)	(3)	(4)	(5)	(6)	(7)
277	8.33	0.36	7.3058	2.65	Single	γ Dor
2842	7.98	0.33	9.2480	2.81	Single	overlap
6260	**8.22**	**0.33**	**8.4356**	**2.85**	**Single**	**overlap**
6568A	6.91	0.32	15.5557	2.87	SB1	overlap
7169A	7.45	0.33	10.9329	2.64	VB,SB2	overlap
8801A	6.42	0.29	18.5729	2.76	VB	overlap
9365A	8.23	0.30	8.2760	2.82	VB	overlap
17163	6.03	0.32	20.5836	2.60	Single	overlap
17310A	7.78	0.36	9.7080	2.72	SB1	γ Dor
18995	6.72	0.35	13.8995	2.43	Single	γ Dor
19649	**7.64**	**0.39**	**8.9117**	**2.39**	**Single**	γ Dor
19684A	6.95	0.27	9.5066	1.84	SB1	overlap
23874A	8.46	0.33	8.1588	3.02	VB,SB2	γ Dor
25906A	7.08	0.33	14.8586	2.94	SB1?	γ Dor
28819	**7.78**	**0.33**	**9.5602**	**2.68**	**Single**	**overlap**
31550	6.73	0.34	17.6567	2.96	Single	γ Dor
32348A	7.40	0.30	10.1384	2.43	SB2	overlap
34415A	**8.47**	**0.30:**	**8.2170**	**3.04**	**SB2**	**overlap**
38309Aa	6.24	0.33	18.2940	2.55	VB,SB2	overlap
40745	6.20	0.35	16.2691	2.26	Single	overlap
41448	7.59	0.30	10.9328	2.78	Single	overlap
41547A	6.41	0.35	17.6712	2.65	SB2	γ Dor
45638	6.57	0.29	17.4589	2.78	Single	overlap
48271	7.47	0.32	8.7951	2.19	Single	overlap
49015A	7.04	0.34	13.5802	2.70	VB	γ Dor
58431	**7.84**	**0.30**	**9.7168**	**2.78**	**Single**	**overlap**
62196A	7.67	0.32	14.2407	3.44	SB1	γ Dor
62454A	7.42	0.33	12.2902	2.87	SB2	overlap
63436	7.43	0.35	12.6018	2.93	Single	γ Dor
64729	7.56	0.34	10.4318	2.65	Single	γ Dor
65526	6.97	0.29	15.0493	2.86	Single	overlap
68192	7.13	0.36	10.5109	2.24	Single	γ Dor
69682	6.50	0.30	16.3841	2.57	Single	overlap
69715A	7.17	0.31	12.2003	2.60	VB	overlap
70645A	8.11	0.31	8.7357	2.82	SB1	overlap
80731A	8.46	0.32	6.9400	2.67	SB1	overlap
86358A	6.86	0.30	13.3027	2.48	SB2	overlap
89781	7.48	0.32	6.8460	1.66	Single	overlap
99267	6.88	0.31	10.9569	2.08	Single	overlap
99329	6.35	0.33	16.7615	2.47	Single	overlap
100215A	8.06	0.26	8.7739	2.78	SB2	overlap
103751	7.97	0.38	6.7875	2.13	Single	γ Dor
105085A	7.59	0.30	11.3384	2.86	SB2	overlap
105458	7.76	0.29	10.0701	2.78	Single	overlap
108100A	7.26	0.35	11.2222	2.51	SB2	γ Dor
112429	5.22	0.29	34.0276	2.88	Single	overlap
115466	6.89	0.34	13.1191	2.48	Single	overlap
122928	**7.91**	**0.29**	**9.5110**	**2.80**	**Single**	**overlap**
124248	7.17	0.29	13.5206	2.82	Single	overlap
138936	6.55	0.27	17.6161	2.78	Single	overlap
139478	6.69	0.32	16.9751	2.84	Single	overlap
144451A	7.85	0.35	10.1255	2.88	VB	γ Dor
144839	**7.32**	**0.36**	**12.9166**	**2.88**	**SB1**	γ Dor
145005A	7.32	0.30	13.1947	2.92	SB2	overlap
152896	7.54	0.31	10.4221	2.63	Single	overlap
155154	6.17	0.34	21.4701	2.83	Single	γ Dor
160295A	7.86	0.35	10.8491	3.04	SB2	γ Dor
160314	7.74	0.41	9.5694	2.64	Single	γ Dor
165645	6.37	0.27	17.3002	2.56	Single	overlap
166233A	6.03	0.32	18.25[g]	2.34	VB	overlap
167858A	6.61	0.32	16.9430	2.75	SB1	overlap

Table 12
(Continued)

HD[a]	V[b] (mag)	$(B-V)$[b,c] (mag)	π[d] (mas)	M_V[e] (mag)	Duplicity[f]	HR Region
(1)	(2)	(3)	(4)	(5)	(6)	(7)
171244	7.72	0.38	8.1502	2.28	Single	γ Dor
175337	7.36	0.35	12.0598	2.77	Single	γ Dor
182735A	**7.52**	**0.33:**	**12.0673**	**2.93**	**SB2**	γ Dor
187615	7.95	0.31	9.2752	2.79	Single	overlap
195068/9	5.72	0.31	25.5678	2.76	Single	overlap
206043	5.76	0.30	25.4223	2.79	Single	overlap
207223	6.17	0.33	19.8932	2.66	Single	overlap
210719	**7.14**	**0.35**	**12.6927**	**2.66**	**Single**	γ Dor
213617	6.43	0.35	18.6645	2.79	Single	γ Dor
220091A	6.80	0.31	15.6059	2.77	VB,SB2	overlap
221866B	8.47	0.29	7.6373	2.88	SB2	overlap
224945	6.92	0.28	15.4553	2.87	Single	overlap

Notes.
[a] Bold indicates a new γ Dor variable star discovered in this paper.
[b] Magnitudes from the Tycho-2 catalog converted to the Johnson system.
[c] A colon indicates greater uncertainty than usual.
[d] From the Gaia DR2 parallax catalog.
[e] Computed from the V magnitude in Col. 2 and the parallax in Col. 4.
[f] SB1 = single-lined binary, SB2 = double-lined binary, VB = visual binary.
[g] We have adopted the recomputed Hipparcos parallax (van Leeuwen 2007), which is listed by *Simbad* in its basic data section and is nearly 80% larger than the DR2 value.

Section 4.1 (above), and the resulting photometric data were uniformly analyzed by the method described in Section 4.2 (above). In particular, we analyzed the frequency spectra of all 73 stars over the frequency range of 0.01–30.0 day^{-1}, which includes the observed frequencies of both δ Sct and γ Dor stars. We note that our ground-based observations are sensitive to peak-to-peak amplitudes down to a couple mmag at best.

Of the 73 γ Dor stars in this sample, 25 lie exclusively in the γ Dor region of the H-R diagram while 48 lie in the δ Sct/γ Dor overlap region. Of the 48 stars in the overlap region, we find only one δ Sct/γ Dor hybrid, namely HD 8801 (Henry & Fekel 2005), the first hybrid pulsator to be discovered. Its δ Sct frequencies are 7.9024, 8.4200, 20.1402, and 20.6714 day^{-1} with peak-to-peak amplitudes of 4.5, 5.4, 4.1, and 3.1 mmag, respectively. The γ Dor frequencies are 2.4795 and 2.8384 day^{-1} with amplitudes of 10.7 and 4.9 mmag.

Thus, for our ground-based observations of γ Dor stars in the overlap region of the δ Sct and γ Dor variables, we find an incidence of δ Sct/γ Dor hybrids of only 1 in 48 or 2.1%. We also note that no δ Sct frequencies were found in the 25 γ Dor variables that lie exclusively in the γ Dor region of the H-R diagram. In addition to HD 8801, a small number of δ Sct/γ Dor hybrids have recently been discovered in other ground-based observations (e.g., Poretti et al. 2005; Zhang et al. 2012; Koen et al. 2016). Therefore, the incidence of δ Sct/γ Dor hybrids is only a few percent for ground-based observations.

Given that many δ Sct stars have amplitudes less than 2 mmag (e.g., Rodriguez et al. 2000), ground-based observations alone must significantly underestimate the incidence of hybrid variables. Photometric observations from the Kepler (Borucki et al. 2010) and TESS (Ricker et al. 2015) space missions have clearly shown this to be the case. Grigahcene et al. (2010) analyzed early observations from Kepler Quarter 0 and Quarter 1 and found a large number of δ Sct/γ Dor hybrids with frequency spectra so rich that there were practically no pure δ Sct or γ Dor variables. They proposed a new classification scheme that takes into account both the amplitudes and frequencies of each star and categorized 234 stars as δ Sct, γ Dor, δ Sct/γ Dor, or γ Dor/δ Sct hybrids. More recently, Balona et al. (2015) conducted a search for δ Sct stars among 20,000 stars in the Kepler field with known stellar parameters. With Kepler's amplitude limit of about 50 ppm, they were able to identify over 2000 δ Sct stars in their sample, but restricted further analysis to 403 δ Sct stars observed in the short-cadence (SC) mode to avoid the chance of frequency misidentification. They detected the presence of low-frequency γ Dor pulsations in all 403 δ Sct stars, which they claimed "rendered meaningless the concept of δ Sct/γ Dor hybrids."

Initial results from the TESS mission confirm a high incidence of δ Sct/γ Dor hybrids. Antoci et al. (2019) conducted an analysis of 117 previously known variable stars in the classical instability strip with data from TESS Sectors 1 and 2. They found 66 δ Sct stars, 3 γ Dor stars, 22 hybrids, and 26 stars with amplitudes too small to classify. However, the photometric precision of TESS is not as good as Kepler; an analysis of 80 days of nearly uninterrupted observations of the prototype γ Doradus itself by Christophe et al. (2020) found 21 frequencies, including the six previously known from ground-based observations. The smallest frequencies detected had amplitudes of about 0.5 mmag, roughly a factor of 10 larger than the smallest amplitudes detected by Kepler.

The large incidence of δ Sct/γ Dor hybrids with many pulsation frequencies, along with the precise, long-term, continuous light curves now available from space missions, are enabling more detailed asteroseismic modeling and understanding of the pulsation mechanisms operating in these stars. While the high-frequency, low-radial order p modes operating in δ Sct stars are driven by the opacity mechanism in the He II ionization zone as well as by turbulent pressure (e.g., Antoci et al. 2014) and the low-frequency g modes in γ Dor stars are

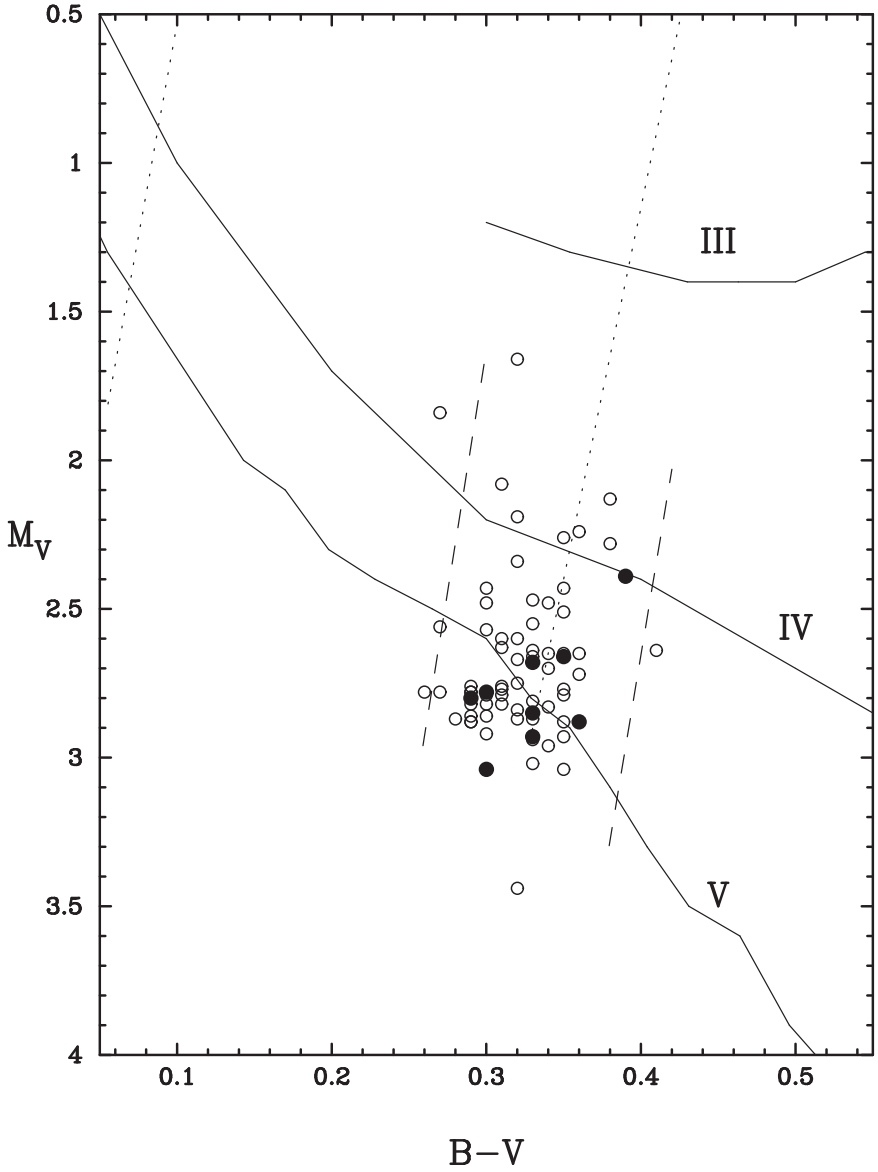

Figure 25. H-R diagram showing the location of the 9 new γ Dor variables discovered in this paper (filled circles) along with the 64 γ Dor stars previously discovered or confirmed in our APT program (open circles), taken from the list of 73 stars in Table 12. The dotted lines indicate the boundaries of the δ Sct instability strip, converted from those of Breger (2000). The dashed lines show the observed limits of the γ Dor variables taken from Fekel et al. (2003) and unchanged in this paper.

excited by convective flux modulation (Guzik et al. 2000), it is not known whether a single excitation mechanism might be responsible for both the p and g modes in hybrid stars (Balona et al. 2015). Bowman & Kurtz (2018) examined a large number of stars observed by Kepler that show pulsations in the δ Sct regime and found that a significant fraction of the main-sequence variables lie outside the theoretical instability strip. Grigahcene et al. (2010) list a number of outstanding questions that asteroseismic studies of δ Sct/γ Dor hybrids may help to answer: (1) why are there so many hybrids when theory predicts hybrids to lie only in the overlapping region of the δ Sct and γ Dor instability strips? (2) why are intermediate frequencies between δ Sct and γ Dor ranges detected whereas theory predicts a frequency gap? (3) can we discover other pulsation mechanisms in these stars? (4) will they help us distinguish between different explanations for the red edge of the δ Sct instability strip? (5) why are there stars that lie within the δ Sct and γ Dor strips that show no periodic variability, even at the micromagnitude precisions of the Kepler observations? Finally, we note that Aerts (2021) reviews the "*renaissance* of stellar evolution theory" over the past decade brought about by the combination of high-quality, space-based light curves of these stars, improved data analysis techniques for the light curves, and more detailed models of stellar structure that together allow the measurement of stellar structure and energy transport from core to surface of stars with a wide variety of masses, ages, and metallicities.

We thank Lou Boyd for his long-term support of the automatic telescopes at Fairborn Observatory. We also appreciate the support of Daryl Willmarth during our coudé feed observing runs at KPNO. Astronomy at Tennessee State University has enjoyed many years of support from NASA, NSF, Tennessee State University, and the State of Tennessee

through its Centers of Excellence program. We thank the referee for several useful suggestions that improved the paper. This work made use of data from the European Space Agency (ESA) Gaia mission (Gaia Collaboration et al. 2016) DR2 catalog (Gaia Collaboration et al. 2018) as well as the SIMBAD database, operated at CDS, Strasbourg, France.

Facilities: KPNO, Fairborn Observatory.

ORCID iDs

Gregory W. Henry https://orcid.org/0000-0003-4155-8513
Francis C. Fekel https://orcid.org/0000-0002-9413-3896

References

Abt, H. A., & Morrell, N. I. 1995, ApJS, 99, 135
Aerts, C. 2021, RvMP, 93, 5001
Antoci, V., Cunha, M., Houdek, G., et al. 2014, ApJ, 796, 118
Antoci, V., Cunha, M. S., Bowman, D. M., et al. 2019, MNRAS, 490, 4040
Baglin, A., Auvergne, M., Boisnard, L., et al. 2006, in Proc. 36th COSPAR Scientific Assembly (Beijing: CDROM), 3749
Balona, L. A., Daszynska-Daszkiewicz, J., & Pamyatnykh, A. A. 2015, MNRAS, 452, 3073
Barker, E. S., Evans, D. S., & Laing, J. D. 1967, RGOB, 130, 355
Bopp, B. W., Evans, D. S., Laing, J. D., & Deeming, T. J. 1970, MNRAS, 147, 355
Borucki, W. J., Koch, D., Basri, G., et al. 2010, Sci, 327, 977
Bowman, D. M., & Kurtz, D. W. 2018, MNRAS, 476, 3169
Breger, M. 2000, in ASP Conf. Ser. 210, Delta Scuti and Related Stars, ed. M. Breger & M. H. Montgomery (San Francisco, CA: ASP), 3
Christophe, S., Antoci, V., Brunsden, E., Ouazzani, R.-M., & Salmon, S. J. A. J. 2020, in Proc. Conf. on Stars and their Variability Observed from Space, ed. C. Neiner et al. (Vienna: Univ. Vienna), 101
Crawford, D. L. 1975, AJ, 80, 955
Demarque, P., Woo, J.-H., Kim, Y.-C., & Yi, S. K. 2004, ApJS, 155, 667
Drilling, J. S. 1973, AJ, 78, 44
Duflot, M., Fehrenbach, C., Mannone, C., Burnage, R., & Genty, V. 1992, A&AS, 94, 479
Duflot, M., Fehrenbach, C., Mannone, C., & Genty, V. 1990, A&AS, 83, 251
Eaton, J. A., Henry, G. W., & Fekel, F. C. 2003, in The Future of Small Telescopes in the New Millennium, Volume II: The Telescopes We Use, ed. T. D. Oswalt (Dordrecht: Kluwer), 189
Eaton, J. A., & Williamson, M. H. 2007, PASP, 119, 886
Feigelson, E. D., & Kriss, G. A. 1983, AJ, 88, 431
Fekel, F. C., & Griffin, R. F. 2011, Obs, 131, 283
Fekel, F. C., Rajavi, S., Muterspaugh, M. W., & Williamson, M. H. 2013, AJ, 145, 111
Fekel, F. C., Tomkin, J., & Williamson, M. H. 2009, AJ, 137, 3900
Fekel, F. C., Warner, P. B., & Kaye, A. B. 2003, AJ, 125, 2196
Frankowski, A., Jancart, S., & Jorissen, A. 2007, A&A, 464, 377
Gaia Collaboration, Brown, A. G. A., et al. 2018, A&A, 616, A1
Gaia Collaboration, Prusti, T., et al. 2016, A&A, 595, A1
Giridhar, S., Goswami, A., Kunder, A., Muneer, S., & Selvakumar, G. 2013, A&A, 556, A121
Gontcharov, G. A. 2006, AstL, 32, 11
Gray, D. F. 1992, The Observation and Analysis of Stellar Photospheres (Cambridge: Cambridge Univ. Press), 431
Grenier, S., Baylac, M. O., Rolland, L., et al. 1999, A&AS, 137, 451
Grigahcene, A., Antoci, V., Balona, L., et al. 2010, ApJL, 713, L192
Guzik, J. A., Kaye, A. B., Bradley, P. A., Cox, A. N., & Neuforge, C. 2000, ApJL, 542, L57
Handler, G., & Shobbrook, R. R. 2002, MNRAS, 333, 251
Harlan, E. A. 1969, AJ, 74, 916
Hauck, B., & Mermilliod, M. 1998, A&AS, 129, 431
Henry, G. W. 1995a, in ASP Conf. Ser. 79, Robotic Telescopes: Current Capabilities, Present Developments, and Future Prospects for Automated Astronomy, ed. G. W. Henry & J. A. Eaton (San Francisco, CA: ASP), 37
Henry, G. W. 1995b, in ASP Conf. Ser. 79, Robotic Telescopes: Current Capabilities, Present Developments, and Future Prospects for Automated Astronomy, ed. G. W. Henry & J. A. Eaton (San Francisco, CA: ASP), 44
Henry, G. W. 1999, PASP, 111, 845
Henry, G. W., & Fekel, F. C. 2005, AJ, 129, 2026
Henry, G. W., Fekel, F. C., & Henry, S. M. 2007, AJ, 133, 1421
Henry, G. W., Fekel, F. C., & Henry, S. M. 2011, AJ, 142, 39
Henry, G. W., Fekel, F. C., Henry, S. M., & Hall, D. S. 2000, ApJS, 130, 201
Henry, G. W., Fekel, F. C., Kaye, A. B., & Kaul, A. 2001, AJ, 122, 3383
Hog, E., Fabricius, C., Makarov, V. V., et al. 2000, A&A, 355, L27
Ibanoglu, C., Cakirli, O., & Sipahi, E. 2018, NewA, 62, 70
Jensen, E. L. N., Mathieu, R. D., Donar, A. X., & Dullighan, A. 2004, ApJ, 600, 789
Joshi, S., Mary, D. L., Martinez, P., et al. 2006, A&A, 455, 303
Judge, P. G., Egeland, R., & Henry, G. W. 2020, ApJ, 891, 96
Kaye, A. B., Handler, G., Krisciunas, K., Poretti, E., & Zerbi, F. M. 1999, PASP, 111, 840
Kenyon, S. J., Dobrzycka, D., & Hartmann, L. 1994, AJ, 108, 1872
Kervella, P., Arenou, F., Mignard, F., & Thevenin, F. 2019, A&A, 623, 72
Knude, J. K. 1977, A&AS, 30, 297
Koen, C., & Eyer, L. 2002, MNRAS, 331, 45
Koen, C., van Wyk, F., Laney, C. D., & Kilkenny, D. 2016, MNRAS, 466, 122
Lacy, C. H. S., & Fekel, F. C. 2011, AJ, 142, 185
Mahdi, B. 2008, BASI, 36, 1
Makarov, V. V., & Kaplan, G. H. 2005, AJ, 129, 2420
Mathias, P., Le Contel, J.-M., Chapellier, E., et al. 2004, A&A, 417, 189
Moneti, A., Pipher, J. L., Helfer, H. L., McMillan, R. S., & Perry, M. L. 1984, ApJ, 282, 508
Nordström, B., Stefanik, R. P., Latham, D. W., & Andersen, J. 1997, A&AS, 126, 21
Olsen, E. H. 1983, A&AS, 54, 55
Olsen, E. H. 1984, A&AS, 106, 257
Perry, C. L., & Johnston, L. 1982, ApJS, 50, 451
Pollard, K. R. 2009, in AIP Conf. Ser. 1170, Stellar Pulsation: Challenges for Theory and Observation, ed. J. A. Guzik & P. A. Bradley (Melville, NY: AIP), 455
Poretti, E., Alonso, R., Amado, P. J., et al. 2005, AJ, 129, 2461
Radick, R. R., Lockwood, G. W., Henry, G. W., Hall, J. C., & Pevtsov, A. A. 2018, ApJ, 855, 75
Ricker, G. R., Winn, J. N., Vanderspek, R., et al. 2015, JATIS, 1, 1
Rodriguez, E., Lopez-Gonzalez, M. J., & Lopez de Coca, P. 2000, in ASP Conf. Ser. 210, Delta Scuti and Related Stars, ed. M. Breger & M. H. Montgomery (San Francisco, CA: ASP), 499
Scarfe, C. D., Batten, A. H., & Fletcher, J. M. 1990, PDAO, 18, 21
Slutskij, V. E., Stalbovskij, O. I., & Shevchenko, V. S. 1980, SvAL, 6, 397
Stassun, K. G., Oelkers, R. J., Paegert, M., et al. 2019, AJ, 158, 138
van Leeuwen, F. 2007, A&A, 474, 653
Vaníček, P. 1971, Ap&SS, 12, 10
Wolfe, R. H., Horak, H. G., & Storer, N. W. 1967, in Modern Astrophysics, ed. M. Hack (New York: Gordon and Breach), 251
Young, R. K. 1942, PDDO, 1, 251
Zhang, X. B., Deng, L. C., & Luo, C. Q. 2012, AJ, 144, 141